NASA TECHNICAL NOTE

NASA TN D-5450

C. 1

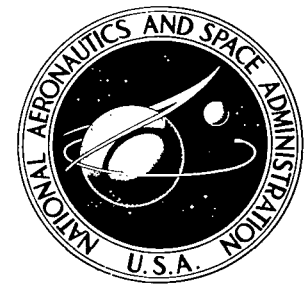

NASA TN D-5450

EFFECTS OF ANGLE OF ATTACK AND BLUNTNESS ON LAMINAR HEATING-RATE DISTRIBUTIONS OF A 15° CONE AT A MACH NUMBER OF 10.6

by Joseph W. Cleary

Ames Research Center
Moffett Field, Calif.

NATIONAL AERONAUTICS AND SPACE ADMINISTRATION • WASHINGTON, D. C. • OCTOBER 1969

1. Report No.	2. Government Accession No.	3. Recipient's Catalog No.
NASA TN D-5450		

4. Title and Subtitle

EFFECTS OF ANGLE OF ATTACK AND BLUNTNESS ON LAMINAR HEATING-RATE DISTRIBUTIONS OF A 15° CONE AT A MACH NUMBER OF 10.6

5. Report Date
October 1969

6. Performing Organization Code

7. Author(s)
Joseph W. Cleary

8. Performing Organization Report No.
A-3324

9. Performing Organization Name and Address
NASA Ames Research Center
Moffett Field, Calif. 94035

10. Work Unit No.
129-01-03-10-00-21

11. Contract or Grant No.

13. Type of Report and Period Covered
Technical Note

12. Sponsoring Agency Name and Address
National Aeronautics and Space Administration
Washington, D. C. 20546

14. Sponsoring Agency Code

15. Supplementary Notes

16. Abstract

Distributions of laminar heating rates are presented from wind-tunnel tests in air at a free-stream Mach number of 10.6 and unit Reynolds numbers from 0.4×10^6 to 1.8×10^6 per foot. Results shown are for angles of attack from 0° to 20° and bluntness ratios from 0 to 0.183. Measurements are included of surface streamlines made by an oil-streak technique. Heating-rate measurements are compared with predictions of similarity theory for $0 \leq \alpha \leq 20°$ and good agreement is indicated.

17. Key Words (Suggested by Author)
Laminar boundary layer
Wind-tunnel tests
Angle of attack
Blunted cones
Laminar-flow theory

18. Distribution Statement
Unclassified - Unlimited

19. Security Classif. (of this report)	20. Security Classif. (of this page)	21. No. of Pages	22. Price*
Unclassified	Unclassified	53	$3.00

*For sale by the Clearinghouse for Federal Scientific and Technical Information
Springfield, Virginia 22151

EFFECTS OF ANGLE OF ATTACK AND BLUNTNESS ON LAMINAR HEATING-RATE DISTRIBUTIONS OF A 15° CONE AT A MACH NUMBER OF 10.6

By Joseph W. Cleary

Ames Research Center

SUMMARY

An investigation was conducted to determine the effects of angle of attack and bluntness on the laminar heating-rate distributions of a 15° semi-apex cone. Heating rates were obtained from wind-tunnel tests in air at a Mach number of 10.6 for free-stream unit Reynolds numbers of 0.4×10^6, 1.2×10^6, and 1.8×10^6 per foot. Included are measurements of surface streamlines made by an oil-streak technique. Results are presented for a range of angles of attack from 0° to 20° and bluntness ratios from 0 to 0.183.

The results show that, at $\alpha = 0^\circ$, increasing bluntness reduced the heating rates and prevented the onset of boundary-layer transition. Bluntness was effective also, at $\alpha > 0^\circ$, in delaying transition on the lee side. On the windward surface, bluntness distorted the flat-plate type heating-rate distributions of the sharp cone. For the bluntest model, the windward heating-rate distributions have minima and maxima that appear related to the pressure distributions.

For $\alpha = 0^\circ$, good agreement of measured heating rates with sharp- and blunted-cone theories was observed. Comparisons for $\alpha > 0^\circ$ demonstrate the general suitability of similarity theory for estimating laminar heating rates on spherical, blunt cones. Comparisons of surface streamlines with inviscid theory show significant effects of bluntness on boundary-layer crossflow; the effects of crossflow on heating rates appear small for the angle-of-attack range of the test.

INTRODUCTION

An evaluation of convective heating is an essential aspect to the proper design of hypersonic vehicles. If lift is employed, heating may prove difficult to estimate even for laminar flows because of the difficulty of evaluating factors relevant to heating, such as boundary-layer profiles, entropy gradients, and streamline geometry. For small angles of attack and bluntness, estimating heating can be simplified since boundary-layer similarity may apply. However, the range of application of boundary-layer similarity is not well defined since it may depend on several parameters, for example, Reynolds number, vehicle shape, and gas composition. There is, therefore, a necessity for measurements of heating rates which designers may use directly and which can serve to verify theoretical estimates.

The purpose of this investigation is to present measurements of the effects of angle of attack and bluntness on laminar heating rates of a 15°

semiapex cone. Results are presented from wind-tunnel tests in air at a Mach number of 10.6. The tests spanned a range of bluntness (ratio of nose radius to base radius) from 0 to 0.183 and angles of attack from 0° to 20°. Results are given for free-stream unit Reynolds numbers of 0.4×10^{6}, 1.2×10^{6}, and 1.8×10^{6} per foot and for a ratio of wall to total temperature of about 0.3. Model base diameter was 1 foot. An oil-streak technique was used to measure the direction of the surface flow. A secondary objective of the present investigation is to compare measurements with simplified approaches to estimating heating. Heating rates for sharp and blunt cones are compared with rates predicted by similarity methods given in references 1 to 4. Surface streamlines relevant to heating are compared with inviscid predictions by the approximate and exact methods of references 5 and 6, respectively. The present results provide in more complete form the preliminary results given in reference 7.

NOTATION

C_p	pressure coefficient, $\left(\frac{p}{p_\infty} - 1\right)\frac{2}{\gamma M_\infty^2}$
c	specific heat
F	pressure function, equation (A10)
G_o	stagnation-point velocity gradient function, equation (5)
g	enthalpy
h	scale factor, equation (A5)
L	sharp-cone length
M	Mach number
m	exponent, equation (6)
Δn	streamline spacing
p	static pressure
q	heat-transfer rate
R	radius of spherical nose
Re	Reynolds number based on model length
s	streamline coordinate
T	temperature
t	time

u	velocity
x,y,z	rectangular coordinates
x,r,φ	body-axis cylindrical coordinates
x_o,r_o	wind-axis coordinates
α	angle of attack
β	pressure-gradient parameter, equation (4)
γ	ratio of specific heats
δ	cone semiapex angle
λ	polar angle of the nose (sketch (c))
ρ	density
τ	thickness
ψ	angle of streamlines to cone elements (sketch (d))
ω	inclination of cone elements to the free-stream velocity

Subscripts

b	model base
e	edge of boundary layer
i	sphere-cone tangent point
max	maximum
min	minimum
o	stagnation point
s	sharp cone
sl	stagnation line
T	transition
w	wall
∞	free stream

Superscripts

*	unit value
~	bluntest model
'	differentiation
—	effective value

APPARATUS AND TESTS

Facility

The tests were conducted in air in the Ames 3.5-Foot Hypersonic Wind Tunnel. This facility is a blowdown tunnel with a steady-state testing time of about 1 to 2 minutes. The operation of the tunnel and the model support mechanism is essentially automatic and data are recorded on magnetic tape. The tests were made at a Mach number of 10.6 and a total temperature of 2000° R. Free-stream unit Reynolds numbers of the tests were 0.4×10^6, 1.2×10^6, and 1.8×10^6 per foot corresponding to tunnel total pressures of 400, 1200, and 1800 psia, respectively.

Models and Test Procedure

The models were constructed with thin shells from high purity nickel by an electroforming process. Their wall thickness varied from about 0.10 inch at the nose to 0.03 inch at the base. The model was a 15°-semiapex spherical, blunt cone with a nominal nose radius of 1.10 inches. Inadvertently the nose was electroformed slightly oblate. While the oblateness was not noticeable, accurate measurements with a comparator showed that the radius of curvature at the stagnation point was 1.25 inches. Variations of bluntness ratio, R/r_b, were achieved by attaching appropriate tips to an alternate model. Test bluntness ratios were 0, 0.0625, 0.167, and 0.183 corresponding to nose radii of 0, 0.375, 1.000, and 1.100 inches, respectively. The two extremes of this range of bluntness are displayed by the model configurations in figure 1. Here, the models are shown sting supported in the tunnel and mounted on the side-wall quick-insert device. The models were instrumented with three rows of chromel-alumel thermocouples at circumferential angles φ of 0°, 90°, and 180°. Thermocouple positions and dimensional details of the models are given in figure 2. Thermocouple positions for $R/r_b = 0.167$ are irrelevant and are not given since this bluntness was used exclusively for surface-flow tests. Tests at various φ were made by discrete rotation of the models.

The procedure for heat-transfer tests consisted in: (1) establishing steady-state flow in the tunnel; (2) starting the thermocouple recording equipment; and (3) quickly inserting the model into the flow at the desired angle of attack. Prior to insertion, the model had an isothermal wall temperature of about 530° R. Insertion time was about 0.2 second and the ratio

of wall to total temperature T_w/T_o for the initial part of the temperature-time transient was about 0.27. A similar procedure was used for surface-flow measurements. However, prior to insertion, the model was wrapped with a sheet of paper and coated with a mixture of titanium oxide and oil. The paper was clamped at the fore end by tips that feather-edged to the wrapped surface and at the base by a clamping ring. The models were inserted into the flow for about 3 seconds, which was sufficient to establish steady-state flow patterns. After retraction, the paper was unwrapped and attached to a plane surface to give developed patterns of the flow.

Heat-Transfer Data Reduction

The heat-transfer rates were evaluated by equation (1).

$$q = \rho_w c_w \tau_w \frac{dT_w}{dt} \tag{1}$$

Slopes of the measured temperature versus time curves dT_w/dt were calculated for each thermocouple by a machine-computed finite-difference technique. Accuracy of heat-transfer-rate measurements was assessed from the repeatability of the stagnation-point heating rate of the bluntest model. Several repeated measurements of this heating rate agreed with each other and with theory (ref. 8) within about ±5 percent. For $\alpha = 0^\circ$ repeatability on the conical surface was within about ±6 percent for the three conical rays at $\varphi = 0^\circ$, 90°, and 180°. Since accuracy is related to the level of the heating rate, it is believed that the accuracy of the lowest rates presented is about ±20 percent.

RESULTS AND DISCUSSION

Experimental Heating-Rate Distributions

Measured heating rates for bluntness ratios R/r_b of 0, 0.0625, and 0.183 are presented in tables I, II, and III, respectively. The rates have been normalized by the theoretical stagnation-point heating rate of the bluntest model $\tilde{q}_o$ for each Reynolds number and are tabulated as functions of the sharp-cone axial coordinate x_s/L. Theory of reference 8 was used to estimate $\tilde{q}_o$ and the estimate was based on the measured radius of curvature $\tilde{R}$ = 1.25 inches. Distributions of $q/\tilde{q}_o$ for $Re^*_\infty = 1.2\times10^6$ per foot are presented in graphical form in figure 3 to illustrate the effects of varying φ when the model is at angle of attack. To demonstrate the more significant effects of angle of attack and bluntness, results for the leeward and windward rays ($\varphi = 0^\circ$ and 180°, respectively) are plotted logarithmically in figure 4.

Before considering effects of angle of attack, it is worth investigating the extent to which the distributions are laminar for $\alpha = 0^\circ$. For this case, laminar flat-plate theory predicts that on a logarithmic scale the sharp-cone distributions should conform to a straight line with slope of -0.5. Figure 4 shows that for $R/r_b = 0$, experiment agrees well with this prediction except

over the afterpart of the model at the greater Reynolds numbers where transition of the boundary layer is indicated by increased heating rates. There is also good agreement between experiment and flat-plate theory for small bluntness, $R/r_b = 0.0625$, except when transition occurs near the model base at the greater Reynolds numbers. Since it is apparent from figure 4 that for $R/r_b = 0.183$ the degree of bluntness is sufficient to preclude reasonable comparison with flat-plate theory, distributions for this bluntness are compared with the more applicable predictions of reference 3. The generally good agreement with this theory shown in figure 4 indicates that the flow was laminar for the Reynolds number range of the tests. Furthermore, figure 4 shows that for $\alpha = 0^\circ$ heating rates decreased slightly with increasing bluntness when the boundary layer was laminar. It is concluded that for $\alpha = 0^\circ$, the onset of transition was delayed by either decreasing Reynolds number or increasing bluntness.

Windward heating-rate distributions.- The analysis of windward stagnation-line heating-rate distributions given in reference 9 indicates that if the flow is laminar, these distributions should be straight lines with a slope of -0.5, similar to those for $\alpha = 0^\circ$. Figure 4 shows agreement of experiment with this prediction for $R/r_b = 0$ and 0.0625 at $0 \leq \alpha \leq 20^\circ$ except near the base at small α where transition occurs. On the other hand, the distributions for $R/r_b = 0.183$ are not straight lines but in some cases develop minima and maxima. Reasons for these irregularities in the distributions are not clear, but it appears doubtful that transition is a factor since increasing α delayed the onset of transition for lesser bluntness. Figure 4 indicates that the position of minima and maxima are related in a general way to the loci of minimum and maximum pressure (from ref. 10) shown superimposed on the heating-rate distributions. The windward results indicate that for specific angles of attack and values of x_s/L, $q/\tilde{q}_o$ increased slightly with increasing Reynolds number. Reasons for this increase are not clear.

Leeward heating-rate distributions.- It is apparent from the leeward distributions on figure 4 that increasing α promoted the development of transitional and turbulent flows. Since transition is of general interest, it is worthwhile to show the effects of α more clearly. Therefore, estimates of transition Reynolds number with unit Reynolds number ratio and local Mach number are shown in figure 5. The location of transition was estimated from the heating-rate distributions as indicated in sketch (a). Results for $R/r_b = 0$ (fig. 5(a)) were estimated for flow conditions at the edge of thickened leeward boundary layers using shock angles given in reference 11 and assuming isentropic compression from the shock to the boundary-layer edge. These estimates are slightly greater than preliminary results given in reference 7 because of refinements in the present analysis. Since bluntness ratios are rather small, sharp-cone

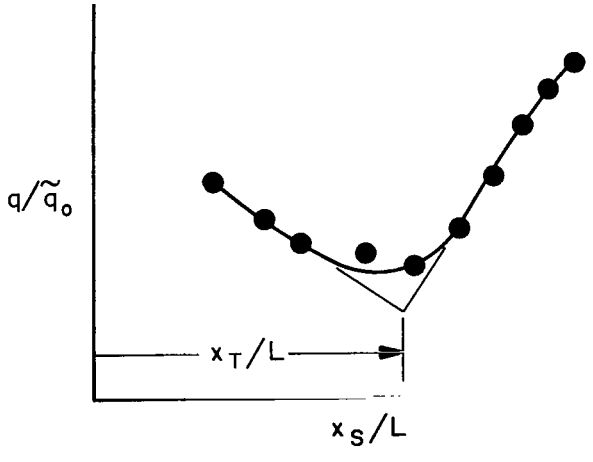

Sketch (a).

unit Reynolds number ratio was used to estimate Re_T for $R/r_b > 0$ (fig. 5(b)) so as to avoid unrealistically low estimates of Re_T. Values of Re^*/Re^*_∞ for sharp and blunt cones shown in figure 5(b) illustrate this effect. However, estimates of local Mach number for the blunt cones are based on isentropic expansion of the flow from the stagnation point to the sharp-cone pressure.

Figure 5 shows that transition Reynolds number for the lee side decreased with increasing angle of attack in agreement with reference 12. Also, as has been observed in references 13 and 14, transition Reynolds number increased with increasing free-stream unit Reynolds number. While, in general, increasing bluntness increased the transition Reynolds number, a reversal in this trend is indicated at the higher angles of attack as bluntness increased from 0 to 0.0625.

Comparison of Experiment With Theory

Before experimental heating rates are compared with theory for $\alpha > 0^\circ$, it is appropriate to make comparisons at $\alpha = 0^\circ$ since, for axisymmetric flows, laminar theories for both sharp and blunt cones are well established.

Heating-rate comparisons for $\alpha = 0^\circ$.- Measured heating rates normalized by $\tilde{q}_o$ are compared with theoretical predictions in figure 6. Comparisons are made with measurements at $Re^*_\infty = 1.2\times10^6$ per foot as representative of the test Reynolds number range. Theoretical sharp-cone heating rates shown in figure 6(a) have been estimated by applying Mangler's transformation factor, $\sqrt{3}$, to two different flat-plate theories: reference enthalpy theory of reference 1, and more exact solutions of the boundary layer given in reference 2. Surface-flow properties used in the predictions were obtained from an inviscid solution of conical flow by the method of characteristics. Figure 6(a) shows that both theories agree well with experiment over the forward half of the cone length where the flow was laminar. Differences shown between theories are about the same as the small scatter in the data, and it is apparent that either theory is adequate for estimating sharp-cone heating rates.

Comparisons of blunt-cone theory with experiment are shown in figures 6(b) and 6(c) for bluntness ratios of 0.0625 and 0.183, respectively. Similarity theory from reference 4, as expressed by equations (2) to (5), was used to predict the distributions shown.

$$\frac{q}{q_o} = \frac{1/2(p/p_o)(u_e/u_\infty)(r/R)(g'_w/g'_{w_o})}{G_o\left[\int_o^{s/R} (p/p_o)(u_e/u_\infty)(r/R)^2\, d(s/R)\right]^{1/2}} \tag{2}$$

where

$$g'_w/g'_{w_o} = 0.936 + 0.90\sqrt{\beta} \tag{3}$$

$$\beta = \frac{2\{[d(u_e/u_\infty)]/[d(s/R)]\}}{(p/p_o)(u_e/u_\infty)^2(r/R)^2}\left[\int_o^{s/R} \frac{p}{p_o}\frac{u_e}{u_\infty}\left(\frac{r}{R}\right)^2 d\left(\frac{s}{R}\right)\right] \tag{4}$$

and

$$G_o = \{[d(u_e/u_\infty)]/d(s/R)\}_o^{1/2} \tag{5}$$

Pressures, velocities, and velocity gradients used in the theoretical estimates are from a combined blunt-body and method of characteristics solution of the inviscid flow from the program of reference 15. Pressure distributions obtained by this method are shown in references 7 and 10 to agree well with experiment for present test conditions. Theory has been applied in two different ways: (1) by estimating boundary-layer-edge conditions, assuming isentropic expansion of the flow from the stagnation point; and (2) by estimating u_e/u_∞ assuming variable entropy at the boundary-layer edge. For the latter case the local entropy at the edge was evaluated by matching the mass flow in the boundary layer with the flow passing through the curved shock wave. The shock shape was obtained from the aforementioned solution of the inviscid flow. While this procedure is an approximation to the more formidable problem of solving for boundary- and entropy-layer interactions, it does yield a realistic estimate of the effects of entropy gradients.

Figure 6(c) shows that for $R/r_b = 0.183$ the effects of entropy gradients were small, and theory and experiment agree closely. Figure 6(b), on the other hand, indicates that for $R/r_b = 0.0625$ including effects of entropy gradients increased the estimated heating rates about 10 to 15 percent. For this bluntness, experiment agreed better with theory over the forward part of the model when effects of entropy gradients were ignored. While this was not the case over the afterpart of the model, the experimental results here may have been influenced by incipient transition. It is apparent, therefore, that for $\alpha = 0^\circ$, clearcut indications of significant entropy-gradient effects are not observed experimentally. Attention is directed now to some simple correlations of heating rates.

Sharp-cone correlation for $\alpha > 0^\circ$.- In lieu of an appropriate sharp-cone theory for comparison at $\alpha > 0^\circ$, a correlation of circumferential sharp-cone heating rates is presented. Figure 7 shows this heating-rate correlation with pressure after being normalized by windward stagnation-line values for the same axial position x_s/L. Figure 7(a) correlates heating rates with pressures estimated by the tangent-cone approximation; the correlation in figure 7(b) is similar but the pressures are measured and the range of α is more limited. Symbols denote values of the coordinates for constant φ at $x_s/L = 0.47$, and vertical and horizontal bars designate the variations of heating rates and pressures, respectively, for $0.18 \le x_s/L \le 0.90$. Results are shown for $30^\circ \le \varphi < 180^\circ$ only since heating rates for $\varphi = 0^\circ$ do not correlate well. From figure 7(a) it can be seen that with tangent-cone pressures, sharp-cone heating rates were fairly well correlated by the relation

$$\frac{q}{q_{sl}} = \left(\frac{p}{p_{sl}}\right)^m \tag{6}$$

with $m = 0.667$. While the correlation is not as good if measured pressures are used (fig. 7(b)), it is, nevertheless, fair for a wide range of conditions. It appears that better correlation with tangent-cone pressures may be fortuitous owing to the lower pressures predicted as the lee side is approached. However, since stagnation-line heating rates can be estimated approximately by swept-cylinder theory (see ref. 16, for example) and tangent-cone pressures are readily evaluated, the correlation of figure 7 may prove useful for simplified estimates of heating rates.

As a simpler alternate to the method of reference 16, stagnation-line heating rates can be estimated by equation (7).

$$\frac{q_{sl}}{q_o} = \frac{1}{\sqrt{2}} \sqrt{\frac{R}{r}} \sin \bar{\omega}_{sl} = \left(\frac{R/L}{2 \tan \delta} \frac{1}{x_s/L}\right)^{1/2} \sin \bar{\omega}_{sl} \tag{7}$$

This approximation is based on simple sweep concepts and equations for the stagnation-point heating rates of two-dimensional and axisymmetric bodies. In equation (7) the windward stagnation-line heating rate q_{sl} is normalized by the stagnation-point heating rate of an axisymmetric body of nose radius R; r is the local radius of the cone normal to the cone axis. The angle $\bar{\omega}_{sl}$ represents an empirical correction to the angle between the stagnation line and the free stream to account for differences from sweep theory that accrue when α is not large. As shown in figure 8, equation (7) gives a good estimate of stagnation-line heating rates for present test results when $\bar{\omega}_{sl} = \alpha + \delta - 5^\circ$.

Blunt-cone correlation for $\alpha > 0^\circ$.- Since heating rates were measured for various bluntness ratios and test conditions, the experimental results can be used to test whether there is boundary-layer similarity for cones of different bluntness at angle of attack. For present test conditions, boundary-layer similarity is implied by the heating-rate distribution predicted by equation (8) (see refs. 3 and 17).

$$\frac{q}{q_o} = \frac{\frac{1}{2} \frac{p}{p_o} \frac{u_e}{u_\infty} \frac{\Delta n}{R}}{G_o \left[\int_o^{s/R} \frac{p}{p_o} \frac{u_e}{u_\infty} \left(\frac{\Delta n}{R}\right)^2 d\left(\frac{s}{R}\right)\right]^{1/2}} \tag{8}$$

Sketch (b) illustrates pertinent geometrical aspects of equation (8) when applied to spherically blunted cones. It is evident from the dimensionless

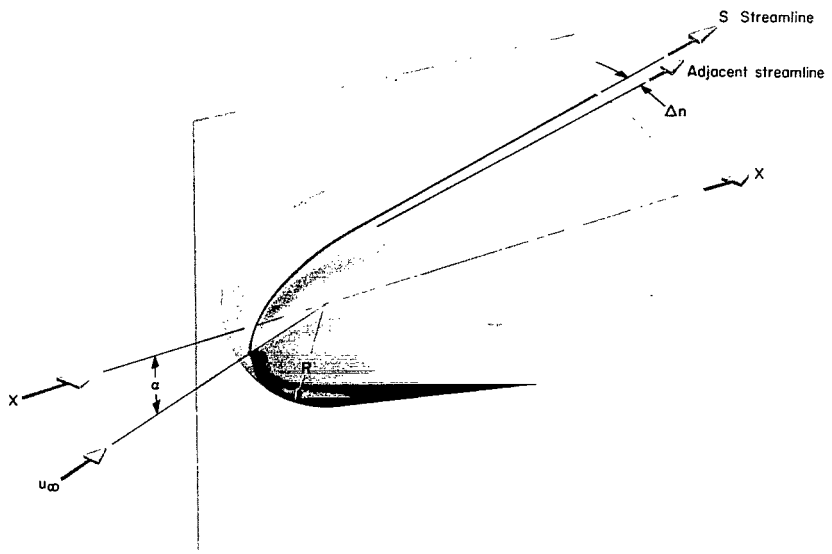

Sketch (b).

form of equation (8) and from sketch (b) that for geometrically similar flows, the predicted distributions of q/q_o as functions of x/R for constant φ are identical. Figure 9 shows a test of similarity by a correlation of present experimental results for $\alpha = 20^o$ using q/q_o and x/R as coordinates. Results shown are from tables II and III and are supplemented by limited unpublished heating-rate distributions for a bluntness ratio of 0.35. In general, good correlation of heating rates is shown in figure 9 for various test conditions. Differences in the distributions for $\varphi = 0^o$ behind the transition point are, of course, irrelevant. The greatest departures from similarity are indicated for $R/r_b = 0.183$ and $\varphi = 180^o$ over the afterpart of the model. Since the entropy layer here is very thin (as demonstrated by pitot-pressure traverses of ref. 11), differences shown are attributed to effects of model scale on boundary-layer and entropy-layer interactions for which equation (8) does not account. In view of the applicability of similarity principles demonstrated by figure 9, measurements will now be compared with similarity theory for $5^o \leq \alpha \leq 20^o$.

Heating-rate comparisons for $\alpha > 0^o$.- Heating rates for blunt cones are inherently more difficult to predict for $\alpha > 0^o$ than for $\alpha = 0^o$ because the geometry of streamlines at the boundary-layer edge must be known. The streamline geometry for inviscid flow can be determined by the accurate three-dimensional method of characteristics as applied, for example, in reference 6. However, this method entails significant computing effort, and computational difficulties may arise for large α. As a simple alternative, the Newtonian method in reference 5 has been selected for estimating streamline geometry.

The suitability of this approach will be scrutinized subsequently when streamlines predicted by theory are compared with those from experiment. With the streamline geometry known, heating rates were predicted by theory of reference 3. Details of the procedure and equations used for present heating-rate estimates are given in appendix A. Assumptions were: (1) the local flow expands isentropically from the stagnation point; and (2) the crossflow component of velocity in the boundary layer is small and can be neglected.

Experimental blunt-cone heating rates normalized by q_o and shown as functions of x/R are compared with theory in figure 10. Theory was applied with measured pressures given in reference 10 and with pressures estimated from modifications to Newtonian theory given by equations (A11) and (A12). In general, theory and experiment are shown to agree well for the angle-of-attack range of the test, $5^\circ \leq \alpha \leq 20^\circ$. It is of interest to observe that with measured pressures, the agreement between theory and experiment is, indeed, improved near the nose where the effects of bluntness on pressures are most important. On the windward ray, $\varphi = 180^\circ$, the differences shown between theory and experiment for $R/r_b = 0.183$ at large x/R are attributed to aforementioned boundary- and entropy-layer interactions.

Surface streamlines.- A comparison of experimental surface streamlines, as indicated by oil streaks, with inviscid theory is shown in figure 11. Here the surface oil streaks have been unwrapped from the cone surface so that quantitative comparisons between experiment and theory can be made. It is tacitly assumed that the oil streaks show the direction of the limiting streamlines at the surface. Theoretical Newtonian streamlines for the blunted cones, shown by solid curves, were predicted by equation (A4) for arbitrary values of φ_i while those for the sharp cone were faired from isoclines computed by equation (B13) for arbitrary values of φ_b. Comparisons are also made in figure 11(c) for $\alpha = 10^\circ$ and $R/r_b = 0$ and 0.167 with surface streamlines computed by the inviscid three-dimensional characteristics procedure given in reference 6. Streamlines for $R/r_b = 0.167$ were forced to cross those predicted by equation (A4) at $x/r = 15$; the sharp cone, crossover point was at the base, $x_s/L = 1$. While the oil streaks clearly indicate streamlines on the windward surface, details of the flow on the lee side are lacking. Apparently, shearing stresses were so small on the lee side, where the pressures were lower, that streaks did not form. Therefore, it is believed that termination of streaks on the lee side is not from flow separation and this is corroborated by the heating-rate measurements. However, for $R/r_b = 0.0625$, figures 11(d) and 11(e) do show some flow details for $\varphi \simeq 0^\circ$ that apparently resulted from turbulence.

From figure 11(c) it can be seen that inviscid streamlines predicted by Newtonian theory agree well with the characteristic solution for the sharp cone but underpredict the crossflow angle, Ψ, for the blunt cone. It is clear from the blunt-cone comparison that the estimates of heating rates, using equation (A4) for streamline geometry, were made along somewhat shorter paths than would have been the case had characteristics theory been used. This applies mainly for φ_i near 90°, however, and not for streamlines nearer the stagnation line where streamlines are fairly well predicted. Also, in view

of the close predictions shown for the sharp cone, it appears that estimates of streamline geometry using equation (A4) would improve as bluntness is decreased.

It is of interest to observe from the experimental oil streaks the progressively steeper crossflow angles, ψ, that result from increasing bluntness for φ near 90° and $\alpha > 0^\circ$. From the characteristic solutions shown in figure 11(c) it is apparent that because of bluntness, inviscid streamlines are inclined at greater ψ than those for the sharp cone. Nevertheless, the angular difference between the oil streaks and the characteristic streamlines is clearly greater for the blunt cone than for the sharp cone. As shown in reference 6, differences between the limiting surface streamlines, as indicated by the oil streaks, and inviscid characteristic streamlines can be accounted for by three-dimensional boundary-layer theory of reference 17.

CONCLUDING REMARKS

Heating rates and surface streamlines from wind-tunnel tests of a 15° semiapex cone at a Mach number of 10.6 are presented. Effects of angle of attack and nose bluntness on heating rates are demonstrated for free-stream unit Reynolds numbers of 0.4×10^6, 1.2×10^6, and 1.8×10^6 per foot. While, in general the heating rates conform to the main aspects of laminar boundary-layer similarity theory, differences are noted at angle of attack that appear to depend on model scale.

For $\alpha = 0^\circ$, increasing bluntness decreases the laminar heating rates and prevents the onset of transition over the afterpart of the model. Increasing bluntness is effective also in preventing transition and turbulent flow that occurs on the lee side of the sharp cone with increasing angle of attack. On the windward side, the flat-plate type distributions of heating rates that characterize laminar boundary layers are distorted by increasing bluntness. For the bluntest model, the heating-rate distributions develop minima and maxima that appear related to the pressure distributions.

For $\alpha = 0^\circ$, good agreement of heating rates with sharp- and blunt-cone theories is shown. Comparisons for $\alpha > 0^\circ$ demonstrate the general suitability of similarity theory for estimating heating rates on blunt cones. Although comparisons of surface-flow streamlines with inviscid theory show that bluntness significantly affects boundary-layer crossflow, the effects of crossflow on heating rates appear small.

Ames Research Center
National Aeronautics and Space Administration
Moffett Field, Calif., 94035, June 11, 1969

APPENDIX A

PROCEDURE FOR ESTIMATING BLUNT-CONE HEATING RATE FOR $\alpha > 0^{\circ}$

Theoretical heating-rate distributions of the present investigation for $\alpha > 0^{\circ}$ were calculated by the method given in reference 5. Using Newtonian theory, reference 5 derives equations for streamlines and scale factors of the axisymmetric analog that are required for the heating-rate estimates. Since the equations in reference 5 are derived in general form, the purpose of this appendix is to give the specific procedure used for present heating-rate estimates. The procedure and equations given apply only to spherically blunted cones.

STREAMLINE GEOMETRY

As shown in sketch (c), streamlines on the nose follow great circles beginning at the stagnation point and crossing the sphere-cone tangent point

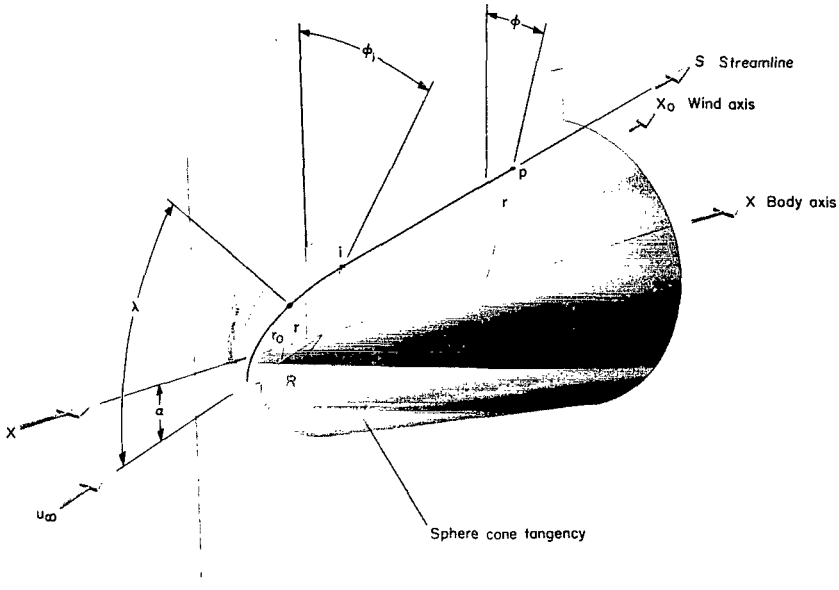

Sketch (c).

at an angle φ_i. The local radius normal to the wind axis to an arbitrary point on a streamline is given by

$$\frac{r_o}{R} = \sin \lambda \tag{A1}$$

where $\lambda = (s/R)$. The body axis coordinate of a point on a streamline is given by

$$\frac{x}{R} = \frac{(1 - \cos \lambda)^2}{1 - \sin \lambda \, (\cot \lambda \cos \alpha - \sin \alpha \cos \varphi_i)} \tag{A2}$$

Values of λ at the sphere-cone tangent point can be estimated from

$$\sin \lambda_i = \cos \delta \left[(\cos \alpha \cos \varphi_i + \tan \delta \sin \alpha)^2 + \sin^2 \varphi_i \right]^{1/2} \tag{A3}$$

For the conical surface, streamlines and scale factors of the axisymmetric analog (ref. 5) are given by equations (A4) and (A5), respectively.

$$\frac{r}{R} = \cos \delta \left(\frac{\tan \varphi_i/2}{\tan \varphi/2} \right)^{\frac{\sin \delta \cos \delta}{\tan \alpha}} \left(\frac{\sin \varphi_i}{\sin \varphi} \right)^{\sin^2 \delta} \tag{A4}$$

$$\frac{h}{R} = \frac{r}{R} \left(\frac{\sin \varphi}{\sin \varphi_i} \right) \left[\frac{\sin^2 \varphi_i + (\cos \varphi_i \cos \alpha + \tan \delta \sin \alpha)^2}{\sin^2 \varphi + (\cos \varphi \cos \alpha + \tan \delta \sin \alpha)^2} \right]^{1/2} \tag{A5}$$

The distance along a streamline is derived in appendix B and can be found by evaluating

$$\frac{s}{R} = \lambda_i + \cos \delta \int_{\varphi}^{\varphi_i} \left\{ 1 + \left[\frac{\cos \delta + \tan \alpha \sin \delta \cos \varphi}{\tan \alpha \sin \varphi} \right]^2 \right\}^{1/2} \frac{r}{R} \, d\varphi \tag{A6}$$

The body axis coordinate is given by

$$\frac{x}{R} = \left(\frac{r}{R} - \frac{1 - \sin \delta}{\cos \delta}\right) \cot \delta \tag{A7}$$

HEATING-RATE DISTRIBUTIONS

In essence, heating rates were evaluated by equation (2) with $g'_w/g'_{w_o} = 1$ and with an assumed isentropic expansion of the local flow from the stagnation point. Over the spherical nose, the appropriate substitution in equation (2) for r/R is r_o/R and over the conical surface, h/R. Substituting (A1) and (A5) in equation (2) $g'_w/g'_{w_o} = 1$ yields respectively for the spherical nose, $0 \leq (r/R) \leq (1 - \sin \delta)$

$$\frac{q}{q_o} = \frac{(1/2) F \sin \lambda}{G_o \left(\int_o^{\lambda} F \sin^2 \lambda \, d\lambda \right)^{1/2}} \tag{A8}$$

and for the conical surface, $(x/R) > (1 - \sin \delta)$

$$\frac{q}{q_o} = \frac{\frac{1}{2} F \left(\frac{h}{R}\right)}{G_o \left\{ \int_o^{\lambda_i} F \sin^2 \lambda \, d\lambda + \cos \delta \int_{\varphi}^{\varphi_i} F \left(\frac{h}{R}\right)^2 \frac{r}{R} \left[1 + \left(\frac{\cos \delta + \tan \alpha \sin \delta \cos \varphi}{\tan \alpha \sin \varphi} \right)^2 \right]^{\frac{1}{2}} d\varphi \right\}^{\frac{1}{2}}} \tag{A9}$$

where F is given by

$$F = \frac{p}{p_o} \left[1 - \left(\frac{p}{p_o} \right)^{(\gamma - 1)/\gamma} \right]^{1/2} \tag{A10}$$

and where, in the denominator of the right side of equation (A9), the integration along streamlines has been transformed by equation (B12) to an

integration over the independent variable, φ. Pressures used in equation (A10) were obtained experimentally (see ref. 10) and were also calculated from modifications to Newtonian theory. For the latter case, pressures over the nose were estimated by

$$\frac{p}{p_o} = \frac{C_{p_o} \cos^2 \lambda + \frac{2}{\gamma M_\infty^2}}{C_{p_o} + \frac{2}{\gamma M_\infty^2}} \tag{A11}$$

and over the conical surface by

$$\frac{p}{p_o} = \frac{C_{p_{sl}} \frac{\sin^2 \omega}{\sin^2 (\alpha + \delta)} + \frac{2}{\gamma M_\infty^2}}{C_{p_o} + \frac{2}{\gamma M_\infty^2}} \tag{A12}$$

where

$$\sin \omega = \sin \delta \cos \alpha - \cos \delta \sin \alpha \cos \varphi \tag{A13}$$

The stagnation-point pressure coefficient, C_{p_o}, was computed from the normal shock relation for air while $C_{p_{sl}}$ was estimated by tangent-cone theory. Stagnation-point velocity gradient was evaluated from a blunt-body solution of the flow by the inverse method of reference 15.

APPENDIX B

DERIVATION OF STREAMLINE LENGTH AND CROSSFLOW ANGLE

Equations are derived for the length of streamlines and the angle of streamlines to cone elements for Newtonian flow over spherically blunted cones.

STREAMLINE LENGTH

The general expression for arc length of a curve in rectangular coordinates is

$$s = \int \left[1 + \left(\frac{dy}{dx} \right)^2 + \left(\frac{dz}{dx} \right)^2 \right]^{1/2} dx \tag{B1}$$

Since streamlines lie on the conical surface, it is expedient to transform equation (B1) to cylindrical coordinates as follows:

$$x = r \cot \delta \tag{B2}$$

$$y = r \sin \varphi \tag{B3}$$

$$z = r \cos \varphi \tag{B4}$$

For constant δ,

$$\frac{dz}{dx} = \frac{dz}{dr} \frac{dr}{dx} = \left(- r \sin \varphi \frac{d\varphi}{dr} + \cos \varphi \right) \tan \delta \tag{B5}$$

$$\frac{dy}{dx} = \frac{dy}{dr} \frac{dr}{dx} = \left(r \cos \frac{d\varphi}{dr} + \sin \varphi \right) \tan \delta \tag{B6}$$

From the substitution of equations (B5) and (B6) in (B1), it follows that on the conical surface

$$s = \int \left[\frac{1}{\sin^2 \delta} + r^2 \left(\frac{d\varphi}{dr} \right)^2 \right]^{1/2} dr \tag{B7}$$

By differentiation of equation (A4) it can be shown that

$$r^2\left(\frac{d\varphi}{dr}\right)^2 = \frac{\tan^2\alpha \sin^2\varphi}{(\sin\delta\cos\delta + \tan\alpha \sin^2\delta\cos\varphi)^2} \tag{B8}$$

and

$$dr = -r\left(\frac{\sin\delta\cos\delta + \tan\alpha \sin^2\delta\cos\varphi}{\tan\alpha \sin\varphi}\right)d\varphi \tag{B9}$$

Substituting (B8) and (B9) in (B7) gives for the streamline length including the nose

$$\frac{s}{R} = \lambda_i + \int_{\varphi}^{\varphi_i}\left[1 + \left(\frac{\cos\delta + \tan\alpha \sin\delta\cos\varphi}{\tan\alpha \sin\varphi}\right)^2\right]^{1/2}\frac{r}{R}\,d\varphi \tag{B10}$$

where r/R is given by equation (A4) as a function of φ.

CROSSFLOW ANGLE

From sketch (d) it can be seen that

$$\sin\psi = -r\frac{d\varphi}{ds} = \frac{\frac{r}{R}}{-\left[\frac{d(s/R)}{d\varphi}\right]} \tag{B11}$$

Differentiating equation (B10) gives

$$-\frac{d(s/R)}{d\varphi} = \left[1 + \left(\frac{\cos\delta + \tan\alpha \sin\delta\cos\varphi}{\tan\alpha \sin\varphi}\right)^2\right]^{1/2}\frac{r}{R} \tag{B12}$$

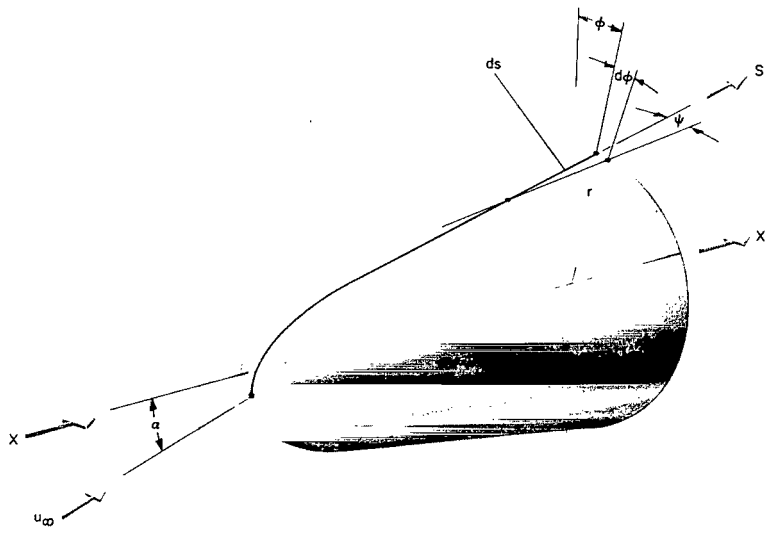

Sketch (d)

Substituting equation (B12) in equation (B11) yields

$$\sin \psi = \frac{1}{\left[1 + \left(\frac{\cos \delta + \tan \alpha \sin \delta \cos \varphi}{\tan \alpha \sin \varphi}\right)^2\right]^{1/2}} \qquad \text{(B13)}$$

Since (B13) is independent of the nose radius, it is evident that it applies to sharp cones as well as blunt.

REFERENCES

1. Eckert, E. R. G.: Engineering Relations for Heat Transfer and Friction in High-Velocity Laminar and Turbulent Boundary-Layer Flow Over Surfaces With Constant Pressure and Temperature. Trans. ASME, vol. 78, no. 6, Aug. 1956, pp. 1273-1283.

2. Van Driest, E. R.: Investigation of Laminar Boundary Layer in Compressible Fluids Using the Crocco Method. NACA TN 2597, 1952.

3. Lees, L.: Laminar Heat Transfer Over Blunt-Nosed Bodies at Hypersonic Flight Speeds. Jet Propulsion, vol. 26, no. 4, April 1956, pp. 259-269.

4. Kemp, Nelson H.; Rose, Peter H.; and Detra, Ralph W.: Laminar Heat Transfer Around Blunt Bodies in Dissociated Air. J. Aerospace Sci., vol. 26, no. 7, July 1959, pp. 421-430.

5. De Jarnette, Fred R.; and Davis, Ruby M.: A Simplified Method for Calculating Laminar Heat Transfer Over Bodies at an Angle of Attack. NASA TN D-4720, 1968.

6. Rakich, John V.; and Cleary, Joseph W.: Theoretical and Experimental Study of Supersonic Steady Flow Around Inclined Bodies of Revolution. AIAA Paper 69-187, 7th Aerospace Sciences Meeting, Jan. 20-22, 1969.

7. Cleary, Joseph W.: Effects of Angle of Attack and Nose Bluntness on the Hypersonic Flow Over Cones. AIAA Paper 66-414, 4th Aerospace Sciences Meeting, June 27-29, 1966.

8. Fay, J. A.; and Riddell, F. R.: Theory of Stagnation Point Heat Transfer in Dissociated Air. J. Aeron. Sci., vol. 25, no. 2, Feb. 1958, pp. 73-85, 121.

9. Reshotko, Eli: Laminar Boundary Layer With Heat Transfer on a Cone at Angle of Attack in a Supersonic Stream. NACA TN 4152, 1957.

10. Cleary, Joseph W.: An Experimental and Theoretical Investigation of the Pressure Distribution and Flow Fields of Blunted Cones at Hypersonic Mach Numbers. NASA TN D-2969, 1965.

11. Cleary, Joseph W.: Effects of Angle of Attack and Bluntness on the Shock-Layer Properties of a 15° Cone at a Mach Number of 10.6. NASA TN D-4909, 1968.

12. Stetson, Kenneth F.; and Rushton, George H.: A Shock Tunnel Investigation of Boundary-Layer Transition at a Mach = 5.5. AIAA Paper 66-495, 4th Aerospace Sciences Meeting, June 27-29, 1966.

13. Larson, Howard K.; and Keating, Stephen J., Jr.: Transition Reynolds Numbers of Separated Flows at Supersonic Speeds. NASA TN D-349, 1960.

14. Potter, J. Leith; and Whitfield, Jack D.: Effects of Unit Reynolds Number, Nose Bluntness, and Roughness on Boundary Layer Transition. AEDC-TR-60-5, March 1960.

15. Inouye, Mamoru; and Lomax, Harvard: Comparison of Experimental and Numerical Results for the Flow of a Perfect Gas About Blunt-Nosed Bodies. NASA TN D-1426, 1962.

16. Beckwith, Ivan E.: Similar Solutions for the Compressible Boundary Layer on a Yawed Cylinder With Transportation Cooling. NASA TR R-42, 1959.

17. Vaglio-Laurin, Roberto: Laminar Heat Transfer on Blunt-Nosed Bodies in Three-Dimensional Hypersonic Flow. WADC-TN-58-147, ASTIA Doc. AD 155588, May 1958.

TABLE I.- VALUES OF $q/\tilde{q}_o$ FOR $R/r_b = 0$

(a) $Re^*_\infty = 0.4 \times 10^6$ per foot, $\tilde{q}_o = 11.2$ Btu/sq ft sec

	$\alpha = 0^\circ$									
φ, deg	x_s/L									
	0.207	0.250	0.293	0.380	0.466	0.552	0.638	0.724	0.811	0.897
0	0.112	0.0868	0.0816	0.0747	0.0687	0.0651	0.0625	0.0618	0.0575	0.0515
	$\alpha = 5^\circ$									
0	.0596	.0510	.0476	.0383	.0375	.0341	.0298	.0281	.0281	.0341
90	.103	.0962	.0919	.0851	---	.0724	.0664	---	.0570	.0527
180	.159	.145	.132	.121	.108	---	.0945	.0877	.0792	.0766
	$\alpha = 10^\circ$									
0	.0312	.0232	.0152	---	.0125	.0107	.0089	.0071	.0071	.0089
90	.0999	.0946	.0892	.0821	---	.0705	.0634	---	.0544	.0482
180	.204	.185	.170	.154	.139	---	.121	.111	.101	.0937
	$\alpha = 15^\circ$									
0	.0181	.0136	.0091	---	.0109	.0094	.0089	.0136	.0136	.0091
90	.101	.0951	.0888	.0816	---	.0661	.0607	---	.0524	.0453
180	.255	.232	.210	.190	.172	---	.150	.138	.127	.127
	$\alpha = 20^\circ$									
0	.0160	.0133	.0088	---	.0142	.0168	.0129	.0088	.0088	.0178
90	.0975	.0904	.0833	.0762	---	.0621	.0563	---	.0501	.0488
180	.290	.264	.238	.216	.186	---	.168	.152	.137	.133

(b) $Re^*_\infty = 1.2 \times 10^6$ per foot, $\tilde{q}_o = 19.0$ Btu/sq ft sec

	$\alpha = 0^\circ$									
φ, deg	x_s/L									
	0.207	0.250	0.293	0.380	0.466	0.552	0.638	0.724	0.811	0.897
0	0.124	0.110	0.108	0.100	0.0811	0.0832	0.0826	0.0848	0.0887	0.0963
	$\alpha = 5^\circ$									
0	.0641	.0561	.0507	.0481	.0454	.0547	.0668	.0817	.0950	.107
15	.0698	.0620	.0568	.0517	.0465	.0408	.0522	.0661	.0762	.0894
30	.0808	.0707	.0656	.0596	.0505	.0486	.0520	.0556	.0606	.0682
45	.0865	.0778	.0746	.0649	.0541	.0492	.0540	.0568	.0622	.0654
60	.0999	.0917	.0872	.0765	.0612	.0580	.0558	.0586	.0586	.0612
75	.116	.102	.0980	.0870	.0733	.0594	.0615	.0678	.0678	.0708
90	.116	.107	.104	.0982	---	.0789	.0774	---	.0747	.0747
105	.143	.138	.119	.115	.100	.0940	.0910	.0885	.0854	.0925
120	.153	.147	.130	.120	.109	.0999	.0978	.0923	.0897	.0943
135	.162	.148	.136	.121	.110	.102	.0963	.0930	.0897	.0920
150	.179	.163	.147	.135	.121	---	.111	.104	.0960	.101
165	.177	.161	.145	.133	.119	---	.109	.103	.100	.103
180	.178	.162	.157	.134	.126	---	.112	.104	.0986	.107

TABLE I.- VALUES OF $q/\tilde{q}_o$ FOR $R/r_b = 0$

(b) $Re_\infty^* = 1.2 \times 10^6$ per foot, $\tilde{q}_o = 19.0$ Btu/sq ft sec - Concluded

φ, deg	x_s/L									
	0.207	0.250	0.293	0.380	0.466	0.552	0.638	0.724	0.811	0.897
					$\alpha = 10^\circ$					
0	0.0255	0.0226	0.0170	0.0142	0.0186	0.0226	0.0315	0.0385	0.0476	0.0510
15	.0340	.0275	.0225	.0225	.0210	.0215	.0195	.0225	.0250	.0250
30	.0483	.0457	.0411	.0356	.0310	.0270	.0260	.0264	.0290	.0254
45	.0644	.0537	.0483	.0429	.0386	.0346	.0332	.0327	.0349	.0327
60	.0782	.0688	.0652	.0579	.0459	.0500	.0446	.0433	.0433	.0428
75	.0994	.0917	.0862	.0714	.0596	.0505	.0486	.0568	.0510	.0484
90	.124	.110	.108	.100	---	.0833	.0792	---	.0679	.0623
105	.155	.143	.124	.118	.104	.0958	.0928	.0872	.0815	.0815
120	.186	.169	.142	.138	.124	.113	.110	.102	.0980	.0944
135	.206	.187	.168	.153	.137	.125	.119	.111	.105	.103
150	.226	.201	.184	.169	.155	---	.133	.124	.117	.117
165	.235	.214	.193	.174	.158	---	.136	.128	.121	.116
180	.249	.226	.204	.186	.170	---	.147	.136	.130	.127
					$\alpha = 15^\circ$					
0	.0154	.0102	.0102	.0102	.0159	.0182	.0106	.0118	.0118	.0133
15	.0203	.0179	.0153	.0127	.0092	.0082	.0061	.0051	.0040	.0061
30	.0306	.0267	.0232	.0207	.0179	.0150	.0145	.0128	.0153	.0148
45	.0457	.0355	.0330	.0294	.0203	.0205	.0197	.0244	.0203	.0203
60	.0641	.0591	.0532	.0468	.0404	.0311	.0276	.0330	.0301	.0306
75	.0788	.0695	.0666	.0598	.0431	.0390	.0376	.0401	.0401	.0367
90	.117	.105	.0999	.0922	---	.0779	.0717	---	.0620	.0563
105	.155	.138	.122	.116	.104	.0960	.0921	.0842	.0784	.0784
120	.214	.191	.172	.159	.143	.131	.126	.118	.108	.109
135	.237	.216	.190	.176	.157	---	.138	.128	.119	.122
150	.270	.245	.216	.199	.179	---	.157	.147	.138	.136
165	.296	.265	.234	.213	.194	---	.170	.158	.151	.147
180	.299	.272	.241	.221	.197	---	.174	.164	.149	.146
					$\alpha = 20^\circ$					
0	.0213	.0186	.0186	.0186	.0244	.0242	.0236	.0287	.0287	.0276
15	.0130	.0104	.0104	.0063	.0083	.0079	.0076	.0042	.0042	.0052
30	.0200	.0175	.0150	.0100	.0080	.0070	.0060	.0050	.0030	.0050
45	.0307	.0212	.0212	.0186	.0166	.0140	.0110	.0131	.0131	.0100
60	.0479	.0444	.0404	.0328	.0272	.0230	.0196	.0237	.0237	.0202
75	.0797	.0698	.0659	.0574	.0436	.0356	.0325	.0376	.0347	.0347
90	.114	.101	.0971	.0881	---	.0738	.0680	---	.0600	.0557
105	.177	.159	.132	.130	.117	.106	.103	.0931	.0861	.0842
120	.220	.200	.174	.165	.148	.137	.132	.120	.113	.116
135	.275	.250	.220	.204	.187	---	.162	.151	.142	.141
150	.319	.286	.255	.233	.215	---	.188	.175	.165	.163
165	.346	.323	.281	.255	.234	---	.203	.193	.182	.179
180	.344	.326	.282	.260	.234	---	.202	.188	.175	.173

TABLE I.- VALUES OF $q/\tilde{q}_o$ FOR $R/r_b = 0$ - Concluded

(c) $Re_\infty^* = 1.8 \times 10^6$ per foot, $\tilde{q}_o = 22.9$ Btu/sq ft sec

φ, deg	x_s/L									
	0.207	0.250	0.293	0.380	0.466	0.552	0.638	0.724	0.811	0.897
					$\alpha = 0^\circ$					
0	0.134	0.121	0.117	0.109	0.0888	0.0920	0.0980	0.0985	0.115	0.129
					$\alpha = 5^\circ$					
0	.0624	.0559	.0516	.0473	.0594	.0794	.0972	.124	.134	.138
90	.122	.112	.110	.100	.0742	.0860	.0860	---	.0903	.0946
180	.185	.169	.157	.143	.127	---	.120	.116	.112	.129
					$\alpha = 10^\circ$					
0	.0278	.0244	.0222	.0171	.0205	.0313	.0405	.0556	.0628	.0641
90	.122	.113	.111	.103	.0786	.0829	.0786	---	.0718	.0727
180	.244	.220	.203	.184	.167	---	.145	.137	.128	.128
					$\alpha = 15^\circ$					
0	.0213	.0197	.0164	.0135	.0184	.0181	---	.0205	.0205	.0205
90	.121	.111	.107	.0964	.0780	.0796	.0763	---	.0657	.0595
180	.314	.285	.254	.228	.206	---	.180	.170	.160	.160
					$\alpha = 20^\circ$					
0	.0338	.0296	.0253	.0295	.0279	.0278	---	.0296	.0296	.0253
90	.116	.103	.100	.0912	.0658	.0743	.0692	---	.0608	.0549
180	.358	.325	.291	.264	.236	---	.207	.194	.186	.182

TABLE II.- VALUES OF $q/\tilde{q}_o$ FOR $R/r_b = 0.0625$

(a) $Re^*_\infty = 0.4 \times 10^6$ per foot, $\tilde{q}_o = 11.2$ Btu/sq ft sec

	$\alpha = 0^\circ$									
φ, deg	x_s/L									
	0.207	0.250	0.293	0.380	0.466	0.552	0.638	0.724	0.811	0.897
0	0.0998	0.0918	0.0897	---	0.0738	0.0656	0.0630	0.0639	0.0618	0.0549

(b) $Re^*_\infty = 1.2 \times 10^6$ per foot, $\tilde{q}_o = 19.0$ Btu/sq ft sec

	$\alpha = 0^\circ$									
φ, deg										
	0.207	0.250	0.293	0.380	0.466	0.552	0.638	0.724	0.811	0.897
0	0.116	0.105	0.105	0.0977	0.0844	0.0712	0.0712	0.0758	0.0737	0.0763
	$\alpha = 5^\circ$									
0	.0508	.0417	.0356	.0254	.0203	.0142	.0183	.0183	.0142	.0203
15	.0483	.0411	.0411	.0314	.0257	.0234	.0203	.0249	.0249	.0257
30	.0548	.0443	.0418	.0391	.0387	.0397	.0394	.0459	.0459	.0443
45	.0729	.0680	.0640	.0591	.0601	.0560	.0531	.0581	.0566	.0566
60	.0804	.0716	.0716	.0716	.0685	.0605	.0582	.0624	.0588	.0567
75	.0960	.0909	.0884	.0884	.0803	.0690	.0663	.0687	.0641	.0606
90	.112	.107	.116	.110	---	.0904	.0838	---	.0747	.0732
105	.138	.136	.127	.121	.107	.0985	.0934	.0798	.0858	.0838
120	.150	.149	.132	.125	.112	.104	.0990	.0861	.0933	.0959
135	.190	.165	.152	.137	.121	---	.108	.0960	.100	.101
150	.171	.166	.146	.134	.120	.108	.106	.0929	.100	.0965
165	.188	.173	.152	.139	.124	.113	.110	.101	.106	.106
180	.195	.183	.158	.143	.131	---	.118	.112	.110	.112
	$\alpha = 10^\circ$									
0	.0217	.0181	.0155	.0119	.0139	.0139	.0114	.0300	.0300	.0361
15	.0255	.0188	.0162	.0121	.0107	.0082	.0091	.0107	.0107	.0162
30	.0358	.0332	.0317	.0300	.0281	.0303	.0273	.0358	.0358	.0307
45	.0482	.0442	.0442	.0412	.0397	.0381	.0367	.0409	.0357	.0301
60	.0740	.0709	.0678	.0626	.0594	.0507	.0494	.0490	.0459	.0448
75	.0904	.0826	.0881	.0883	.0657	.0552	.0512	.0554	.0524	.0513
90	.119	.113	.113	.102	---	.0821	.0770	---	.0703	.0692
105	.159	.153	.134	.123	.124	.101	.0962	.0822	.0852	.0822
120	.204	.192	.164	.152	.135	.123	.119	.105	.105	.102
135	.222	.202	.177	.163	.145	---	.128	.108	.112	.108
150	.242	.220	.195	.176	.158	.145	.139	.120	.126	.115
165	.237	.218	.189	.174	.158	.143	.140	.118	.125	---
180	.250	.227	.199	.179	.165	.151	.145	.135	.126	.124

TABLE II.- VALUES OF $q/\tilde{q}_o$ FOR $R/r_b = 0.0625$ - Continued

(b) $Re^*_\infty = 1.2 \times 10^6$ per foot, $\tilde{q}_o = 19.0$ Btu/sq ft sec - Concluded

φ, deg	x_s/L									
	0.207	0.250	0.293	0.380	0.466	0.552	0.638	0.724	0.811	0.897
					$\alpha = 15^\circ$					
0	0.0172	0.0172	0.0197	0.0296	0.0325	0.0349	0.0276	0.0414	0.0364	0.0394
15	.0203	.0177	.0147	.0102	.0076	.0077	.0104	.0050	.0050	.0076
30	.0298	.0248	.0224	.0199	.0159	.0157	.0169	.0174	.0174	.0149
45	.0377	.0351	.0327	.0311	.0276	.0279	.0220	.0231	.0211	.0201
60	.0596	.0548	.0527	.0489	.0388	.0322	.0272	.0340	.0314	.0308
75	.0826	.0773	.0773	.0610	.0526	.0465	.0396	.0447	.0400	.0368
90	.131	.120	.116	.100	---	.0818	.0759	---	.0641	.0616
105	.169	.154	.133	.125	.109	.100	.0936	.0768	.0789	.0726
120	.210	.190	.169	.155	.136	.124	.118	.100	.100	.0957
135	.247	.230	.198	.183	.163	---	.143	.121	.124	.115
150	.288	.262	.224	.206	.185	.169	.161	.140	.143	.132
165	.287	---	.254	.218	---	.178	.166	.153	.145	.135
180	.308	.288	.251	.227	.202	.180	.177	.163	.153	---
					$\alpha = 20^\circ$					
0	.0250	.0340	.0451	.0451	.0391	.0380	.0304	.0381	.0350	.0326
15	.0223	.0136	.0163	.0109	.0120	.0130	.0159	.0065	.0065	.0087
30	.0172	.0147	.0128	.0098	.0078	.0087	.0072	.0088	.0059	.0049
45	.0265	.0265	.0245	.0235	.0177	.0174	.0131	.0142	.0137	.0123
60	.0522	.0475	.0443	.0365	.0300	.0254	.0222	.0245	.0224	.0209
75	.0828	.0728	.0702	.0597	.0450	.0379	.0331	.0388	.0356	.0315
90	.126	.111	.107	.0942	---	.0761	.0711	---	.0611	.0601
105	.180	.164	.141	.128	.115	.104	.101	.0812	.0851	.0786
120	.230	.209	.177	.164	.150	.136	.132	.108	.114	.105
135	.286	.262	.228	.206	.184	---	.161	.137	.141	.130
150	.331	.310	.260	.236	.218	.198	.189	.164	.164	.156
165	.338	---	.299	.259	---	.213	.199	.184	.177	.167
180	.377	.343	.290	.269	.238	.214	.206	.193	.181	---

(c) $Re^*_\infty = 1.8 \times 10^6$ per foot, $\tilde{q}_o = 22.9$ Btu/sq ft sec

φ, deg	x_s/L									
	0.207	0.250	0.293	0.380	0.466	0.552	0.638	0.724	0.811	0.897
					$\alpha = 0^\circ$					
0	0.118	0.114	0.110	0.106	0.0957	0.0820	0.0764	0.0787	0.0836	0.0843
					$\alpha = 5^\circ$					
0	.0447	.0532	.0371	.0250	.0205	.0209	.0221	.0189	.0189	.0242
90	.119	.115	.114	.111	---	.0947	.0877	---	.0798	.0786
180	.205	.190	.169	.153	.135	.124	.119	.116	.114	.0987

TABLE II.- VALUES OF $q/\tilde{q}_o$ FOR $R/r_b = 0.0625$ - Concluded

(c) $Re^*_\infty = 1.8 \times 10^6$ per foot, $\tilde{q}_o = 22.9$ Btu/sq ft sec - Concluded

φ, deg	x_s/L									
	0.207	0.250	0.293	0.380	0.466	0.552	0.638	0.724	0.811	0.897
					$\alpha = 10^\circ$					
0	0.0223	0.0142	0.0142	0.0142	0.0194	0.0246	---	0.0357	0.0377	0.0406
90	.128	.124	.124	.110	---	.0884	.0831	---	.0762	.0779
180	.265	.237	.215	.195	.173	.155	.150	.142	.134	.134
					$\alpha = 15^\circ$					
0	.0153	.0185	.0242	.0342	.0403	.0453	---	.0464	.0484	.0443
90	.144	.121	.116	.102	---	.0816	.0770	---	.0681	.0665
180	.324	.297	.256	.208	.206	.181	.177	.167	.157	.158
					$\alpha = 20^\circ$					
0	.0281	.0346	.0482	.0523	.0446	.0394	---	.0394	.0346	.0302
90	.132	.117	.111	.0973	.0772	.0792	.0740	---	.0639	.0603
180	.380	.358	.306	.275	.247	.220	.215	.201	.191	---

TABLE III.- VALUES OF $q/\tilde{q}_o$ FOR $R/r_b = 0.183$

(a) $Re^*_\infty = 0.4 \times 10^6$ per foot, $\tilde{q}_o = 11.2$ Btu/sq ft sec

φ, deg	x_s/L									
	0.207	0.250	0.293	0.380	0.466	0.552	0.638	0.724	0.811	0.897
					$\alpha = 0^\circ$					
0	0.104	0.0845	0.0704	0.0610	---	0.0563	0.0518	0.0516	0.0516	0.0516
					$\alpha = 5^\circ$					
0	.0840	.0748	.0654	.0560	.0280	.0280	.0234	.0186	.0168	.0168
90	.0934	.0794	.0700	.0560	---	.0514	.0514	.0513	.0512	.0467
180	.131	.112	.0934	.0840	---	.0934	.0888	.0840	.0840	.0838
					$\alpha = 15^\circ$					
0	.0430	.0302	.0215	.0156	.0063	.0078	.0098	.0107	.0125	.0195
90	.115	.0742	.0655	.0655	---	.0669	.0689	.0537	.0527	.0517
180	---	---	---	---	---	---	---	---	---	---
					$\alpha = 20^\circ$					
0	.0281	.0191	.0135	.0078	.0056	.0158	.0205	.0242	.0242	.0259
90	---	---	---	---	---	---	---	---	---	---
180	.225	.238	.236	.214	.187	.173	.155	---	.134	.134

(b) $Re^*_\infty = 1.2 \times 10^6$ per foot, $\tilde{q}_o = 19.0$ Btu/sq ft sec

φ, deg	x_s/L									
	0.207	0.250	0.293	0.380	0.466	0.552	0.638	0.724	0.811	0.897
					$\alpha = 0^\circ$					
0	0.122	0.0968	0.0775	0.0692	---	0.0664	0.0636	0.0581	0.0581	0.0554
					$\alpha = 5^\circ$					
0	.0958	.0724	.0549	.0459	---	.0299	.0200	.0200	.0175	.0125
15	.0865	.0664	.0508	.0424	---	.0290	.0248	.0212	.0167	.0112
30	.0911	.0694	.0579	.0434	---	.0326	.0290	.0277	.0239	.0271
45	.0959	.0742	.0553	.0482	---	.0379	.0358	.0348	.0315	.0271
60	.104	.0814	.0625	.0539	---	.0470	.0445	.0445	.0417	.0458
75	.112	.0888	.0699	.0612	---	.0562	.0562	.0592	.0562	.0602
90	.120	.0898	.0799	.0699	.0699	.0698	.0698	.0699	.0699	.0699
105	.114	.0921	.0781	.0725	---	.0714	.0714	.0670	.0709	.0686
120	.137	.117	.104	.0977	.0936	.0992	.0936	---	.0885	.0916
135	.140	.119	.107	.103	.101	.107	.0992	---	.0916	.0975
150	.141	.119	.108	.108	.106	.108	.103	---	.0922	.0922
165	.141	.120	.113	.110	.111	.109	.105	---	.0937	.0949
180	.156	.132	.120	.120	.120	.125	.115	.115	.107	.105

TABLE III.- VALUES OF $q/\tilde{q}_o$ FOR $R/r_b = 0.183$ - Continued

(b) $Re^*_\infty = 1.2 \times 10^6$ per foot, $\tilde{q}_o = 19.0$ Btu/sq ft sec - Concluded

φ, deg	x_s/L									
	0.207	0.250	0.293	0.380	0.466	0.552	0.638	0.724	0.811	0.897
					$\alpha = 10^\circ$					
0	0.0664	0.0487	0.0338	0.0248	0.0166	0.0122	0.0122	0.0122	0.0122	0.0138
15	.0661	.0499	.0358	.0257	---	.0141	.0119	.0100	.0076	.0108
30	.0712	.0540	.0393	.0289	---	.0200	.0189	.0135	.0177	.0174
45	.0798	.0611	.0454	.0373	---	.0284	.0272	.0272	.0247	.0252
60	.0899	.0688	.0528	.0424	---	.0374	.0374	.0374	.0347	.0402
75	.104	.0814	.0643	.0575	---	.0542	.0542	.0573	.0548	.0552
90	.111	.0802	.0776	.0776	.0693	.0693	.0693	.0720	.0720	.0665
105	.127	.106	.0921	.0921	---	.0932	.0921	.0813	.0845	.0796
120	.158	.136	.132	.132	.130	.130	.118	---	.113	.116
135	.177	.156	.147	.161	.151	.144	.129	---	.116	.121
150	.189	.172	.167	.178	.166	.155	.140	---	.135	.142
165	.195	.174	.170	.184	.170	.155	.137	---	.133	.141
180	.189	.177	.177	.183	.166	.155	.144	.144	.144	.149
					$\alpha = 15^\circ$					
0	.0500	.0337	.0258	.0158	.0110	.0110	.0095	.0158	.0205	.0316
15	.0455	.0322	.0222	.0133	---	.0061	.0050	.0050	.0050	.0050
30	.0509	.0373	.0265	.0163	---	.0141	.0119	.0098	.0073	.0070
45	.0629	.0485	.0348	.0258	---	.0223	.0198	.0189	.0177	.0202
60	.0699	.0543	.0409	.0311	---	.0298	.0289	.0306	.0271	.0273
75	.0906	.0710	.0546	.0491	---	.0502	.0513	.0535	.0459	.0437
90	.116	.0894	.0726	.0726	.0685	.0711	.0711	.0621	.0621	.0631
105	.122	.0999	.0888	.0944	---	.0949	.0888	---	.0810	.0810
120	.164	.147	.147	.156	.143	.129	.116	---	.118	.126
135	.210	.194	.189	.202	.177	.166	.148	---	.145	.152
150	.222	.214	.214	.214	.188	.174	.158	---	.154	.162
165	.219	.211	.211	.214	.188	.175	.164	---	.171	.178
180	.250	.247	.247	.242	.208	.197	.192	.187	.179	.184
					$\alpha = 20^\circ$					
0	.0368	.0250	.0153	.0102	.0102	.0215	.0296	.0358	.0409	.0409
15	.0349	.0240	.0164	.0087	---	.0115	.0131	.0131	.0104	.0109
30	.0423	.0302	.0207	.0126	---	.0058	.0048	.0042	.0036	.0035
45	.0511	.0386	.0270	.0215	---	.0155	.0145	.0135	.0120	.0150
60	.0642	.0489	.0346	.0285	---	.0280	.0280	.0280	.0233	.0255
75	.0833	.0634	.0482	.0450	---	.0508	.0477	.0456	.0381	.0425
90	.111	.0868	.0766	.0766	.0741	.0664	.0613	.0587	.0587	.0608
105	.134	.110	.104	.109	---	.100	.0922	---	.0867	.0867
120	.198	.174	.174	.186	.161	.150	.134	---	.128	.132
135	.238	.233	.233	.230	.197	.187	.169	---	.159	.160
150	.277	.277	.277	.260	.224	.211	.191	---	.176	.181
165	.278	.289	.300	.265	.228	.218	.200	---	.191	.191
180	.296	.306	.306	.276	.240	.230	.217	.209	.204	.199

TABLE III.- VALUES OF $q/\tilde{q}_o$ FOR $R/r_b = 0.183$ - Concluded

(c) $Re^*_\infty = 1.8 \times 10^6$ per foot, $\tilde{q}_o = 22.9$ Btu/sq ft sec

φ, deg	x_s/L									
	0.207	0.250	0.293	0.380	0.466	0.552	0.638	0.724	0.811	0.897
$\alpha = 0^\circ$										
0	0.122	0.101	0.0859	0.0752	---	0.0646	0.0645	0.0645	0.0645	0.0601
$\alpha = 5^\circ$										
0	.0971	.0709	.0569	.0407	---	.0263	.0219	.0184	.0184	.0153
90	.122	.0962	.0831	.0700	---	.0612	.0612	.0612	.0634	.0678
180	.166	.149	.131	.131	---	.131	.122	.114	.114	.114
$\alpha = 10^\circ$										
0	.0736	.0541	.0359	.0260	---	.0108	.0095	.0078	.0065	.0065
90	.121	.0909	.0779	.0714	---	.0714	.0714	.0693	.0779	.0758
180	.207	.190	.184	.199	.190	.173	.165	.174	.182	.184
$\alpha = 15^\circ$										
0	.0455	.0347	.0239	.0174	---	.0096	.0130	.0156	.0217	.0217
90	.115	.0898	.0737	.0737	---	.0750	.0750	.0650	.0681	.0693
180	.251	.243	.238	.234	.210	.205	.199	.215	.221	.230
$\alpha = 20^\circ$										
0	.0338	.0211	.0211	.0211	---	.0253	.0296	.0380	.0423	.0423
90	.114	.0908	.0761	.0761	---	.0761	.0697	.0655	.0656	.0710
180	.304	.313	.317	.287	.247	.243	.239	.239	.239	.243

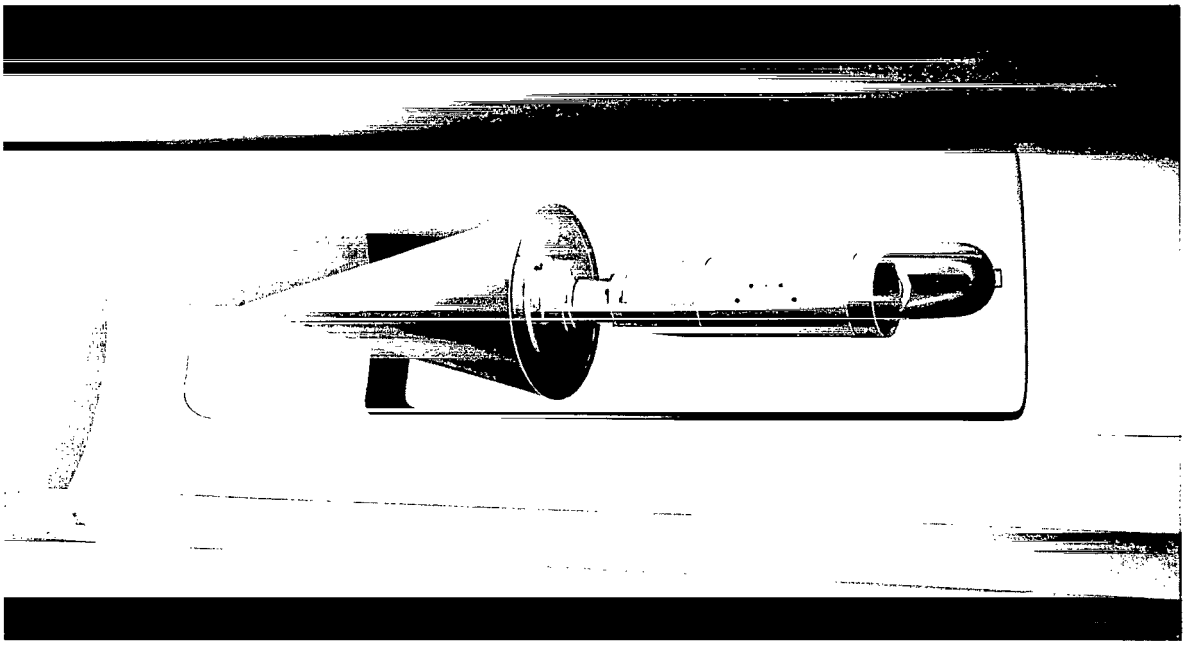

(a) $R/r_b = 0$

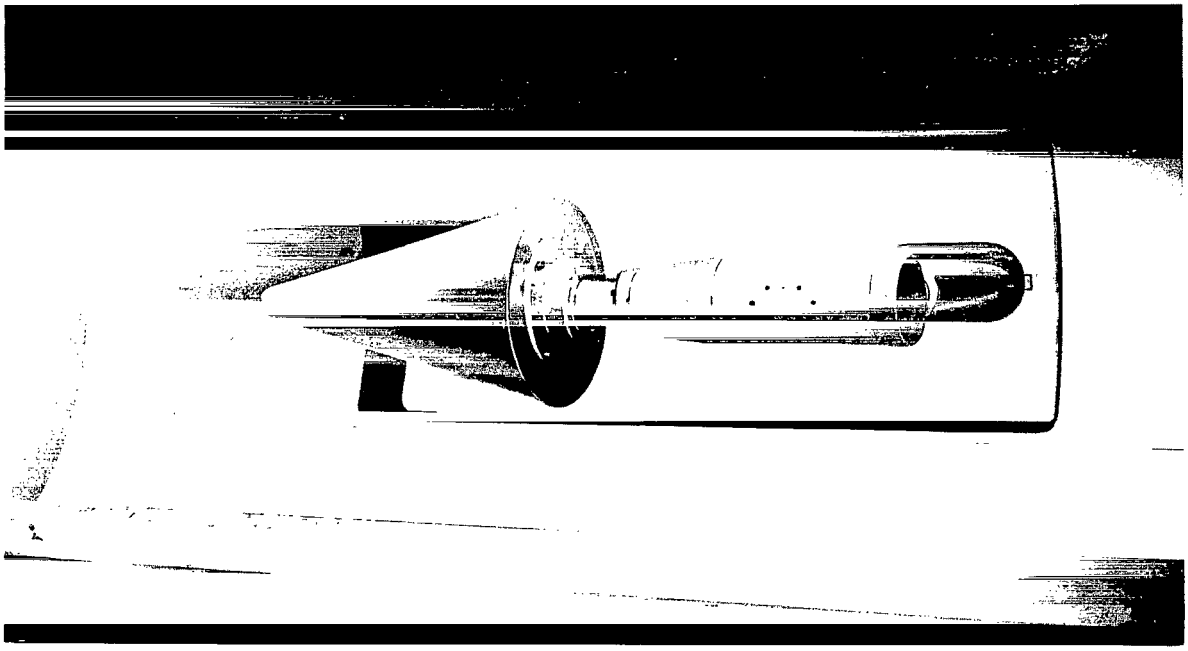

(b) $R/r_b = 0.183$

Figure 1.- Model mounted on the quick insert device in the 3-1/2 foot hypersonic wind tunnel.

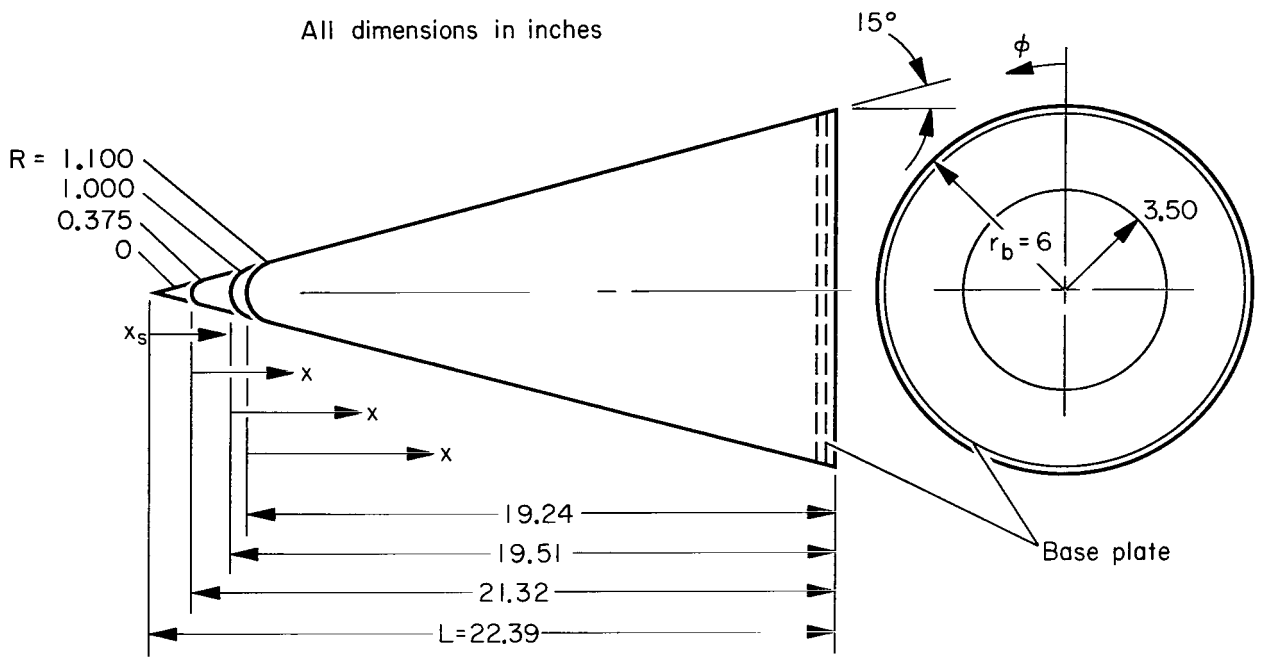

Thermocouple positions		
x_s/L $(R/r_b=0)$	x/R $(R/r_b=0.0625)$	x/R $(R/r_b=0.183)$
0.207	9.49	1.35
.250	12.07	2.23
.293	14.64	3.10
.380	19.81	4.86
.466	24.95	6.62
.552	30.12	8.37
.638	35.27	10.13
.724	40.40	11.89
.811	45.57	13.64
.897	50.70	15.40

Figure 2.- Details of model with alternate tips.

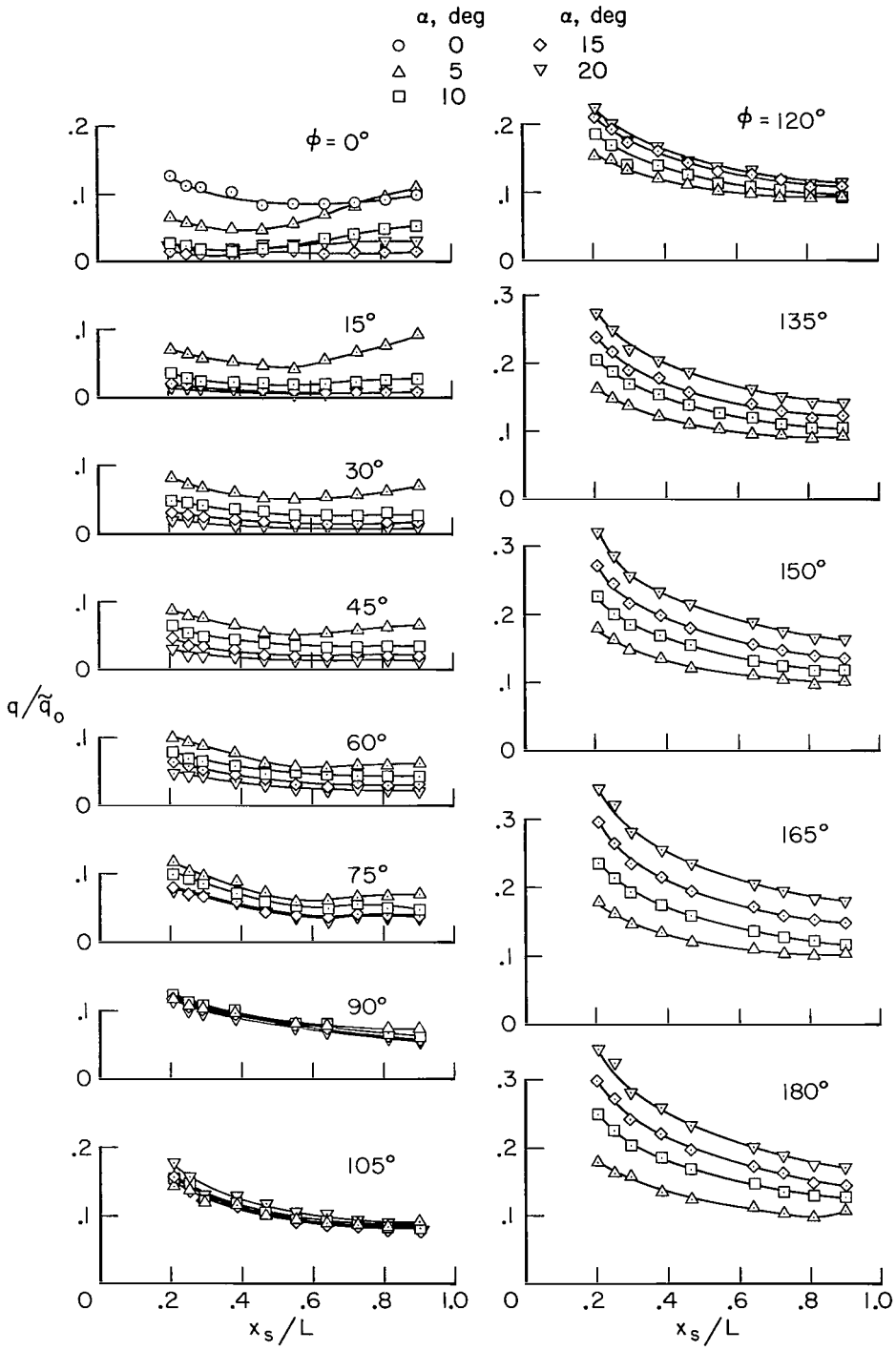

(a) $R/r_b = 0$

Figure 3.- Experimental heating-rate distributions of the 15° conical model; $M_\infty = 10.6$, $Re^*_\infty = 1.2 \times 10^6$ per foot.

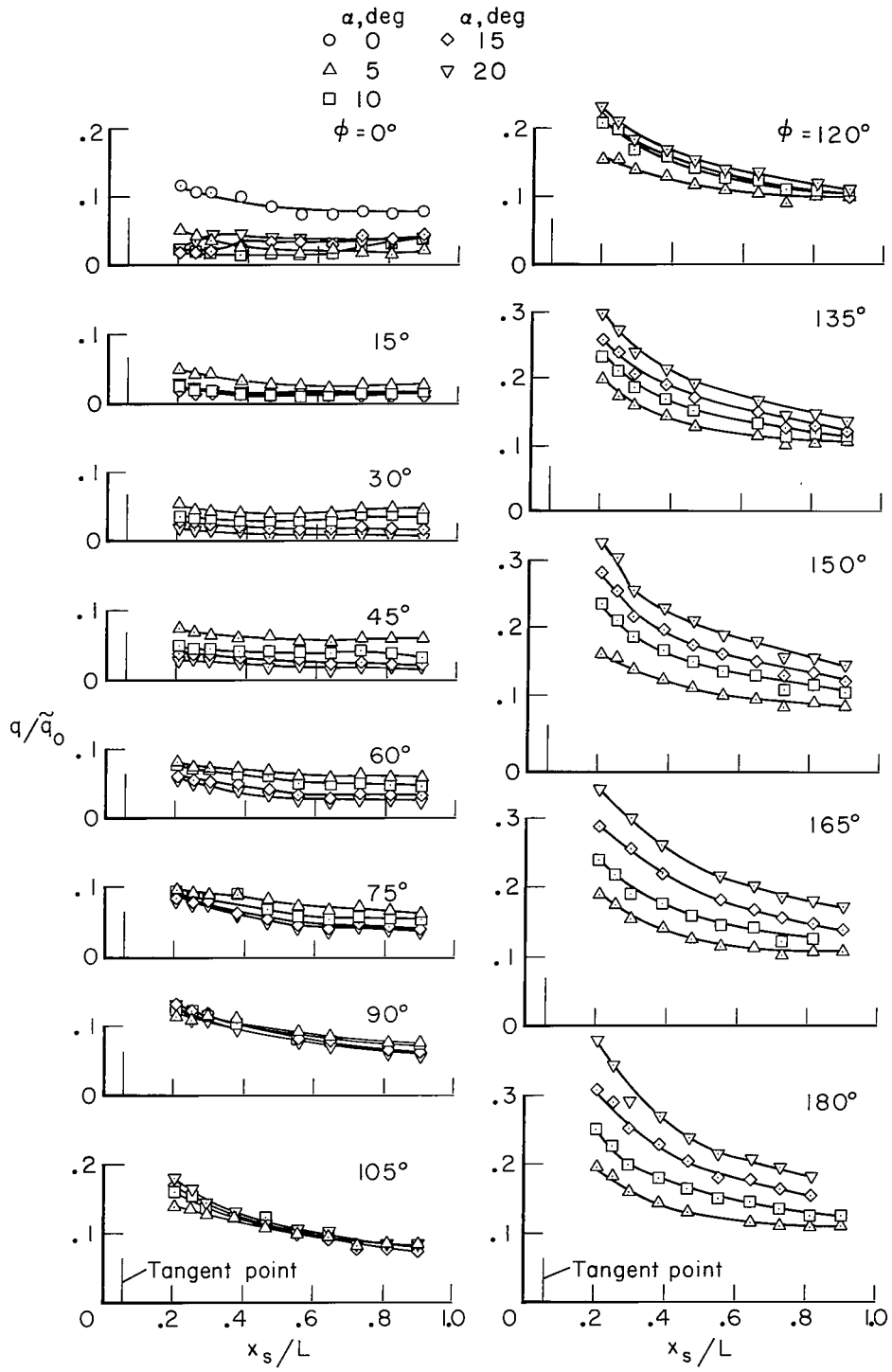

(b) $R/r_b = 0.0625$

Figure 3.- Continued.

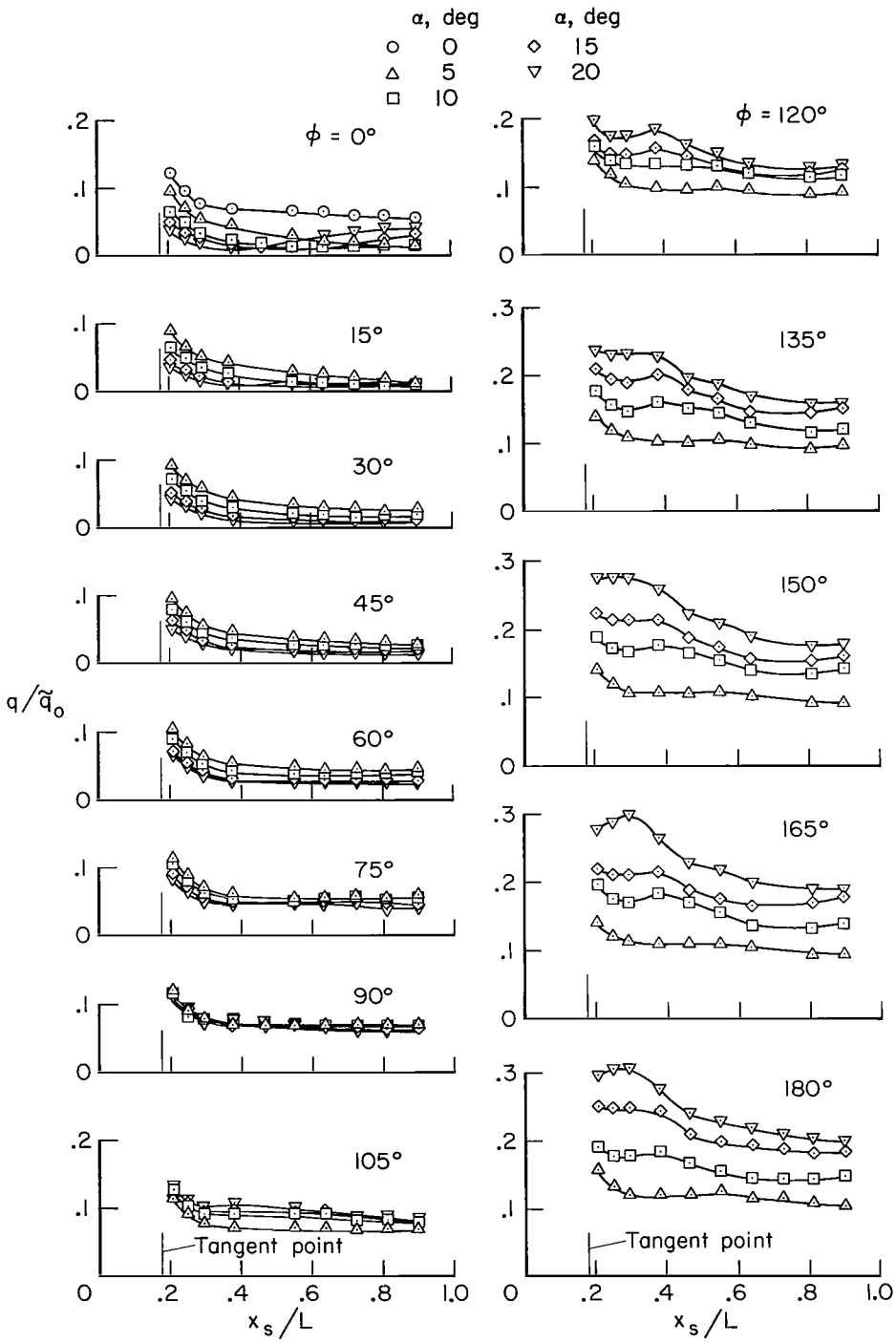

(c) $R/r_b = 0.183$

Figure 3.- Concluded.

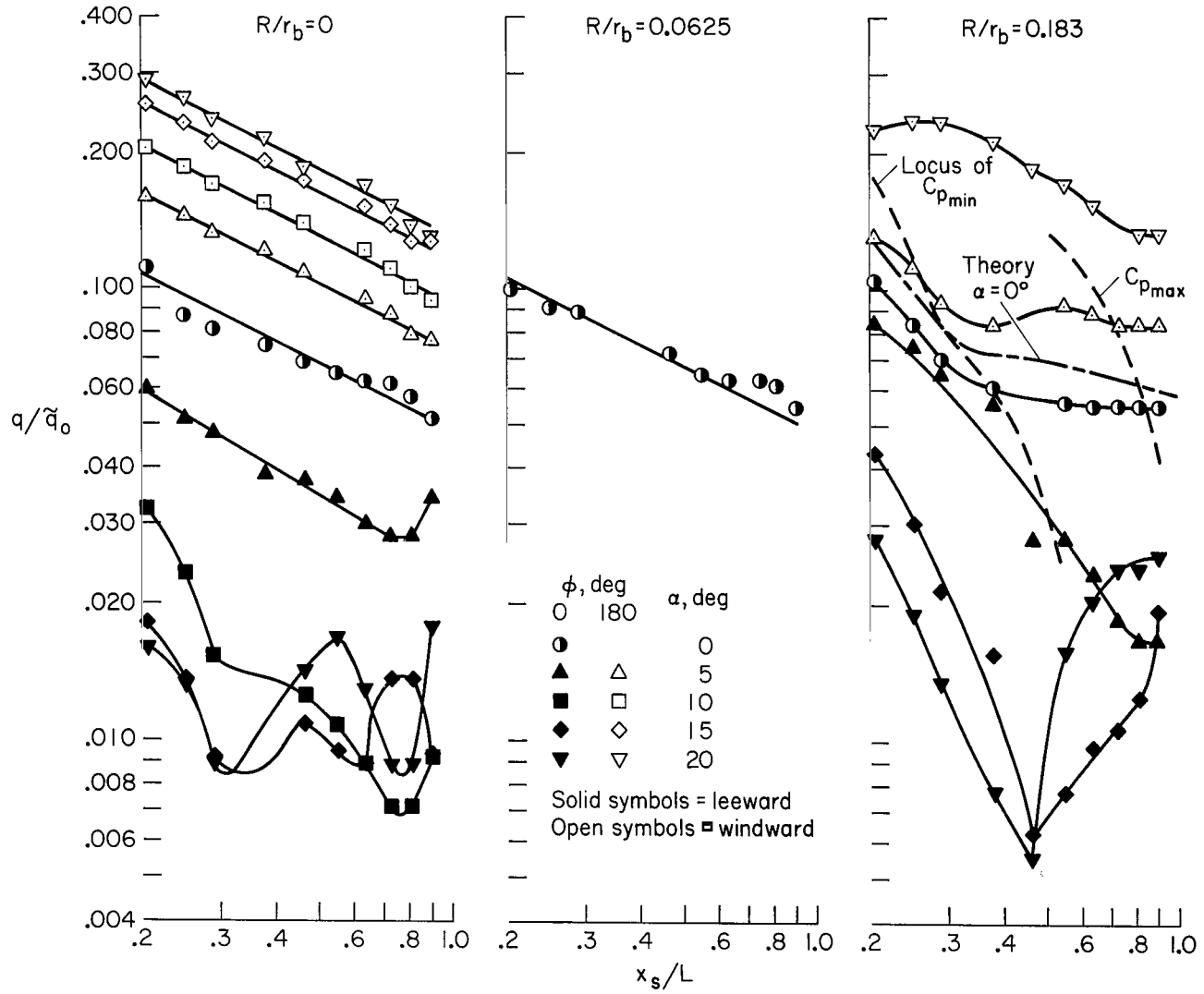

(a) $Re^*_\infty = 0.4\times10^6$ per foot.

Figure 4.- Effects of bluntness and angle of attack on heating-rate distributions for $\phi = 0°$ and $180°$; $M_\infty = 10.6$.

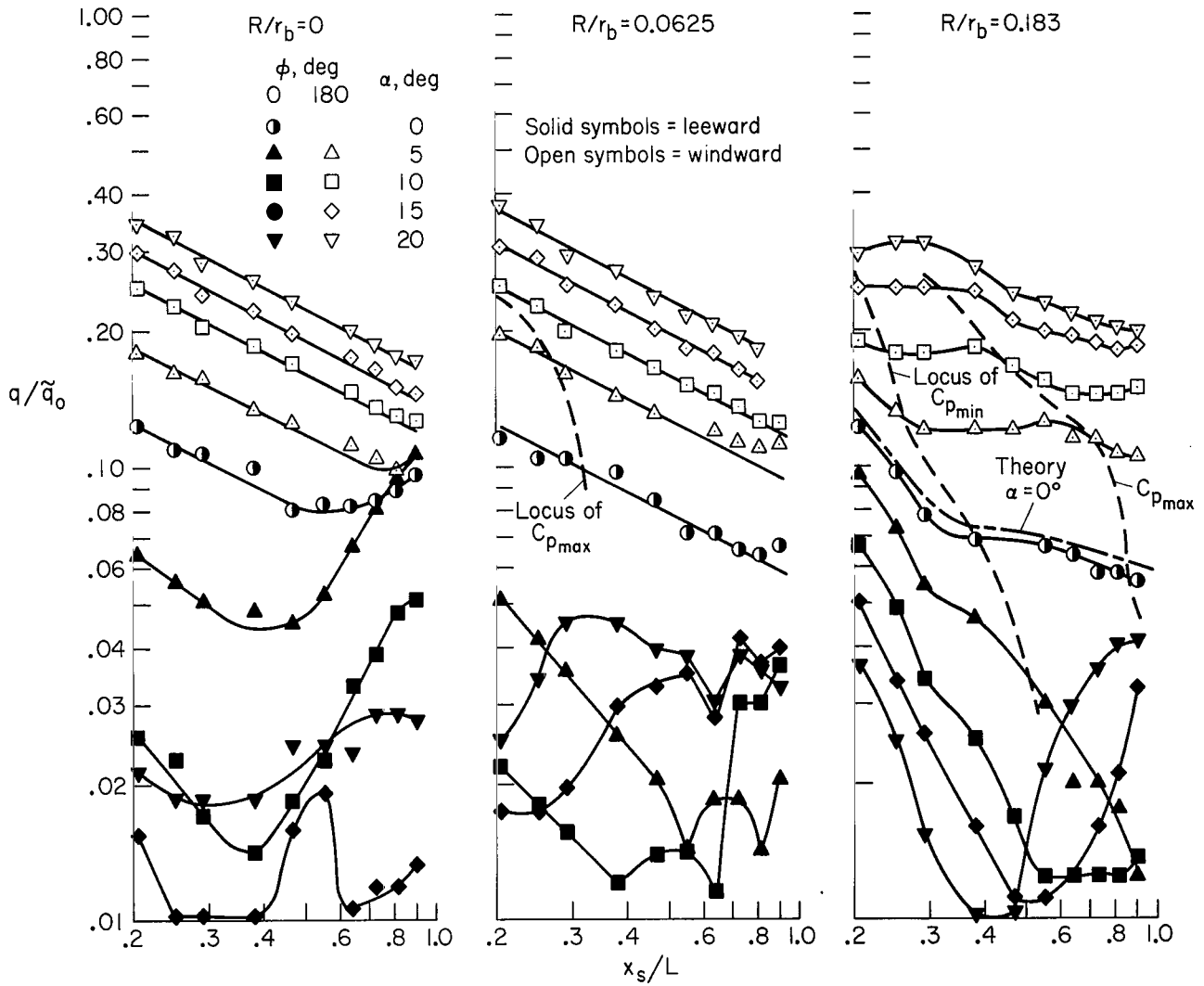

(b) $Re^*_\infty = 1.2\times10^6$ per foot.

Figure 4.- Continued.

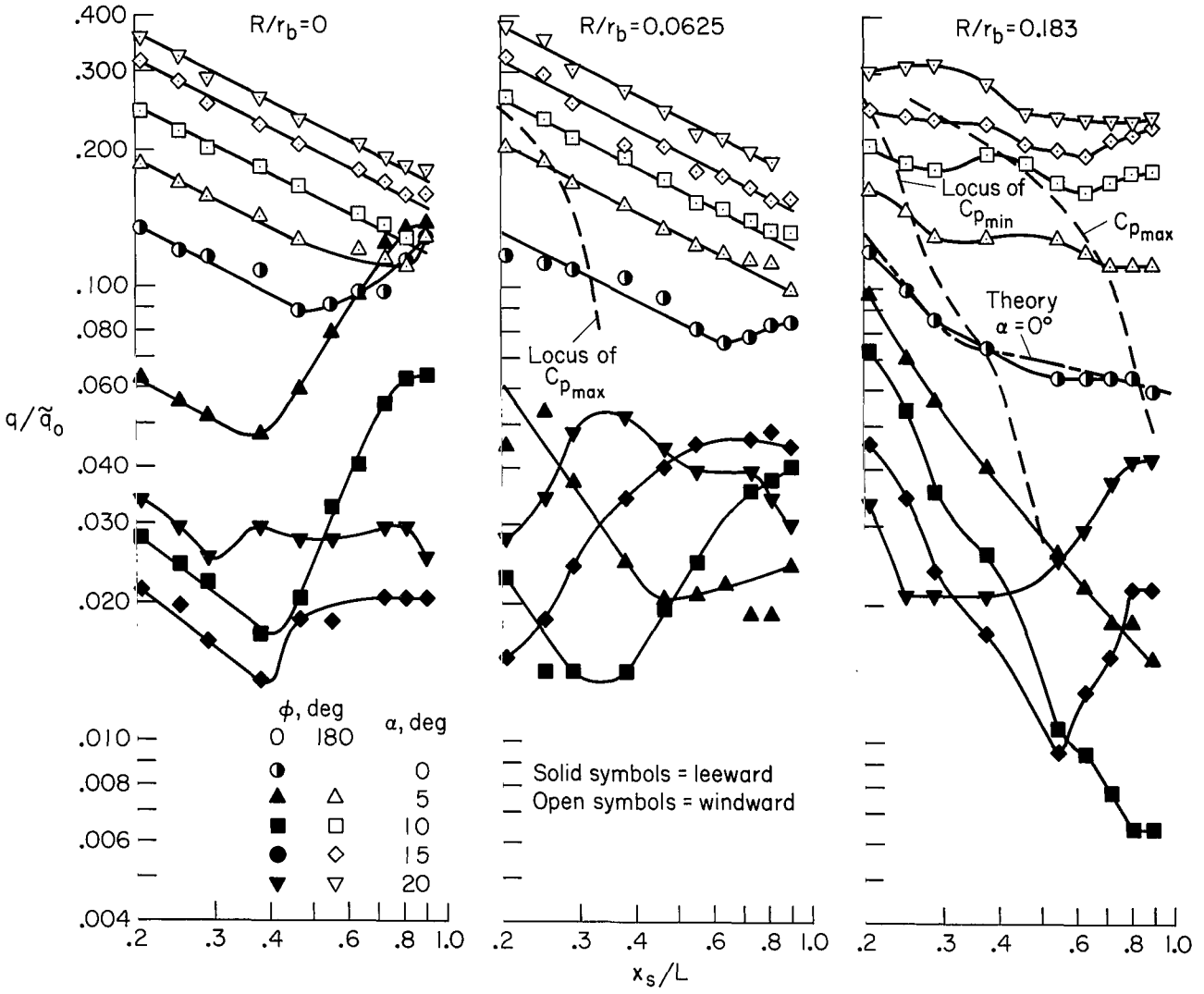

(c) $Re^*_\infty = 1.8\times10^6$ per foot.

Figure 4.- Concluded.

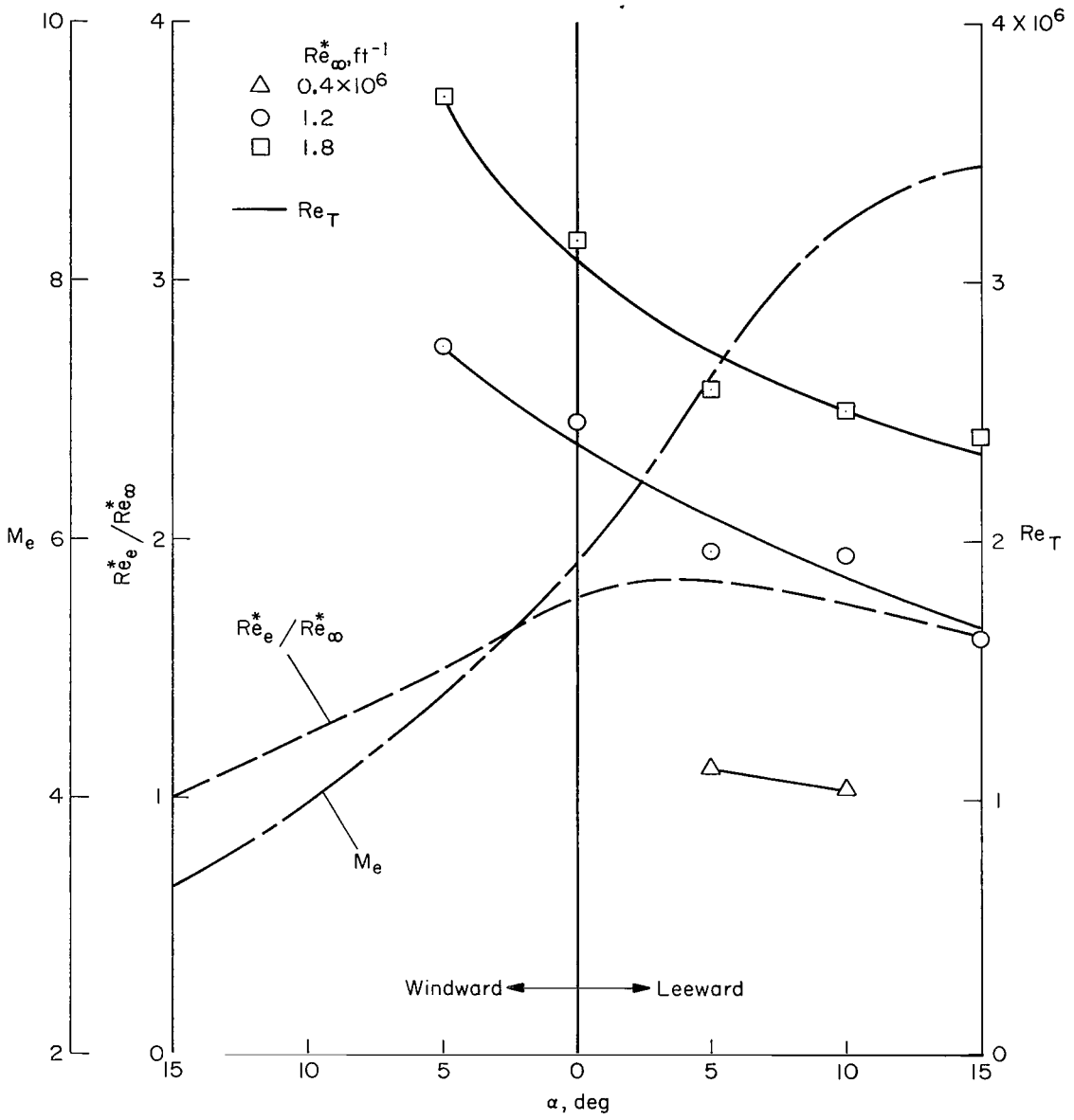

(a) Sharp cone, $R/r_b = 0$.

Figure 5.- Effect of angle of attack on Reynolds number for transition.

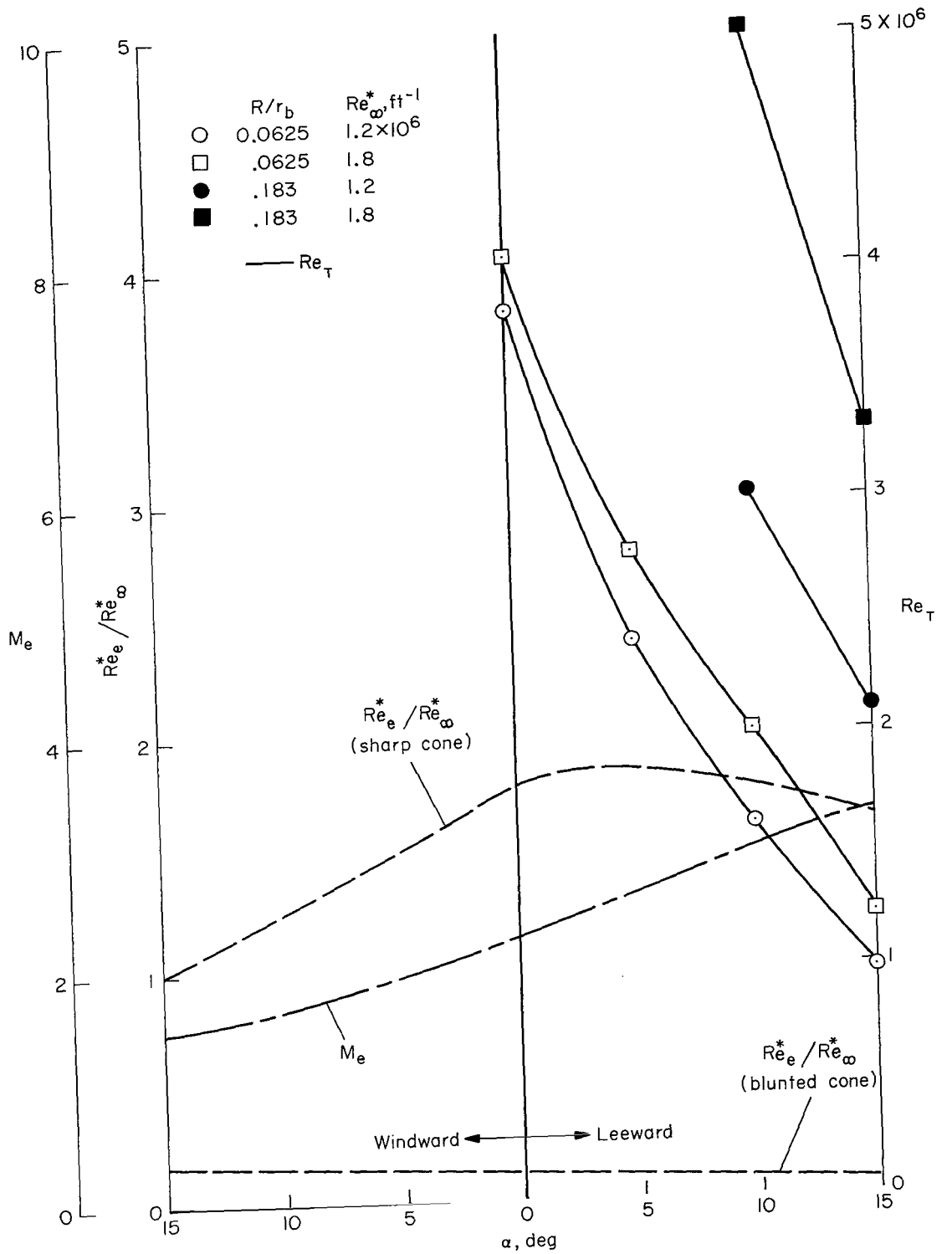

(b) Blunted cones.

Figure 5.- Concluded.

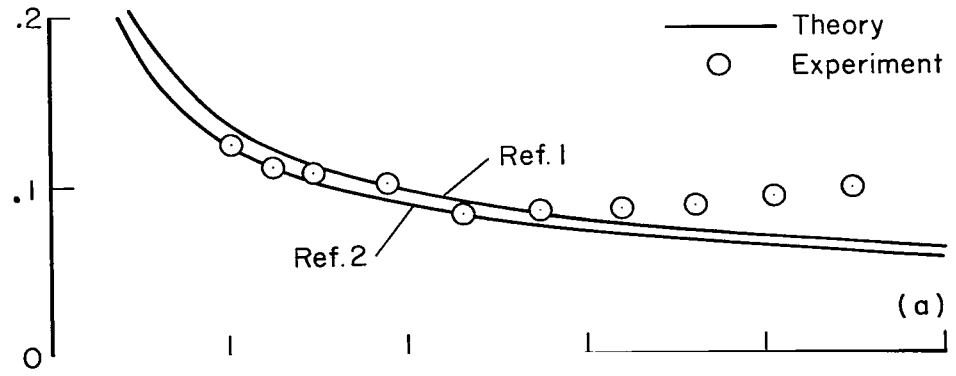

(a) $R/r_b = 0$

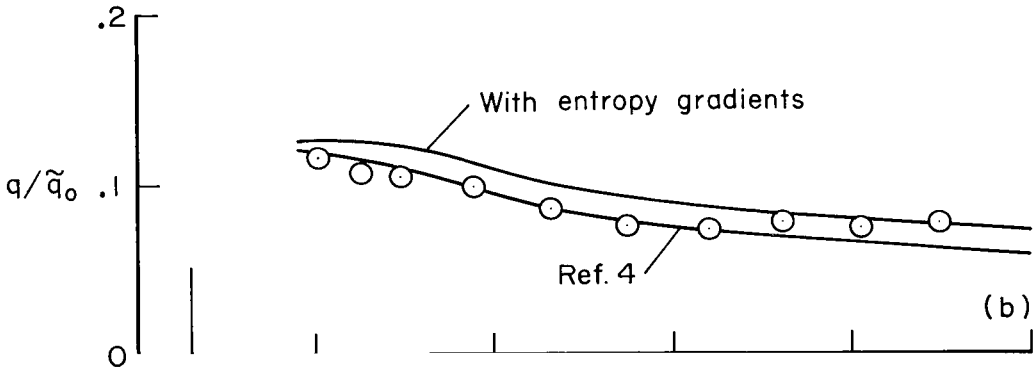

(b) $R/R_b = 0.0625$

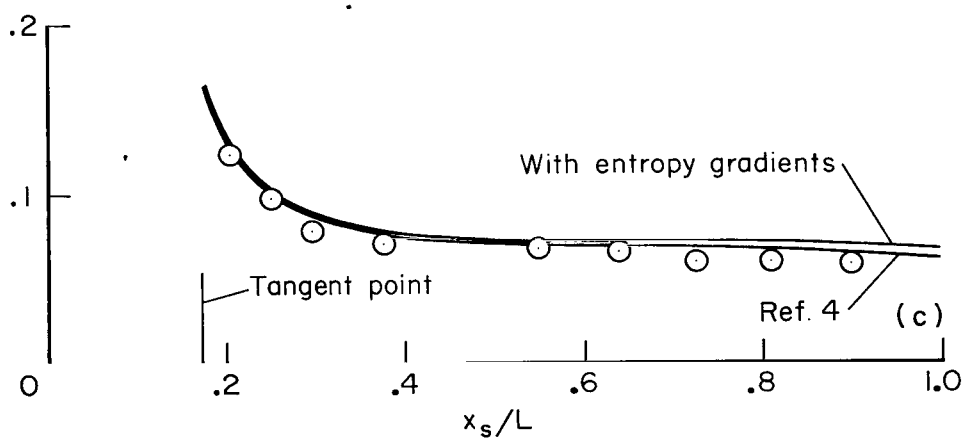

(c) $R/r_b = 0.183$

Figure 6.- Comparison of heating-rate distributions with theory for $\alpha = 0°$; $M_\infty = 10.6$, $Re^*_\infty = 1.2 \times 10^6$ per foot.

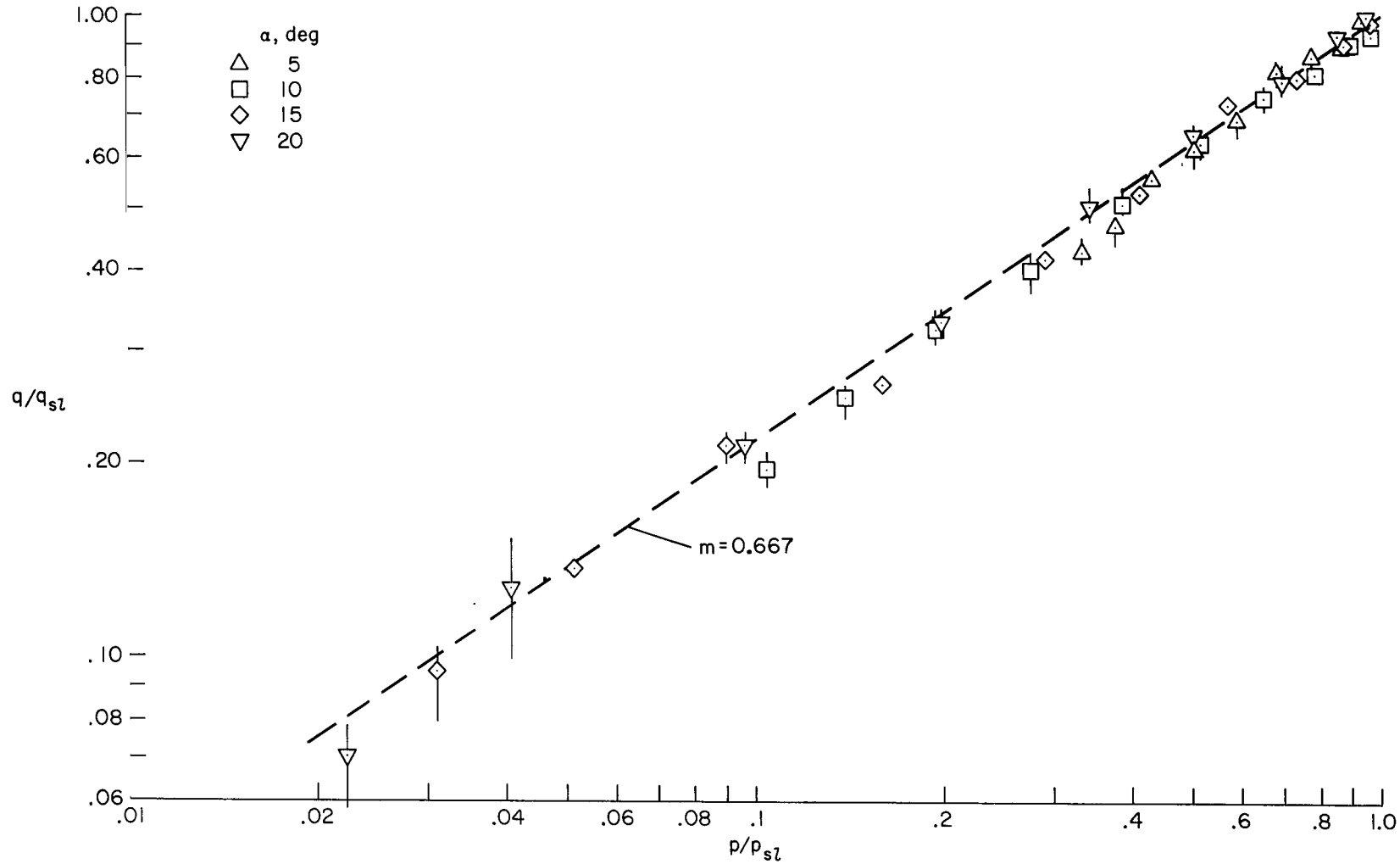

(a) Using tangent-cone pressures.

Figure 7.- Correlation of sharp-cone heating rates; $M_\infty = 10.6$, $Re^*_\infty = 1.2\times10^6$, $\delta = 15°$, $30° \leq \phi \leq 180°$.

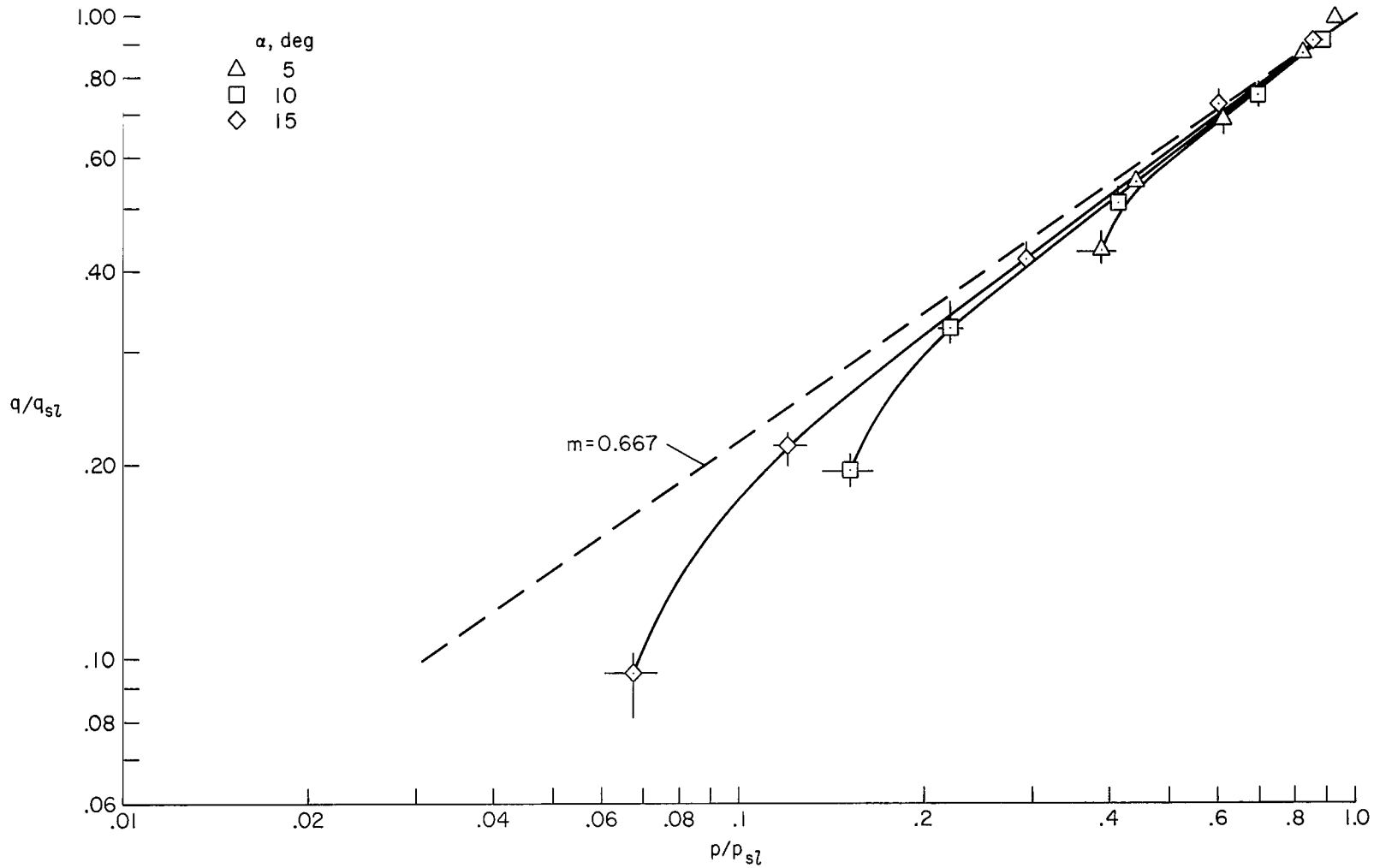

(b) Using measured pressures.

Figure 7.- Concluded.

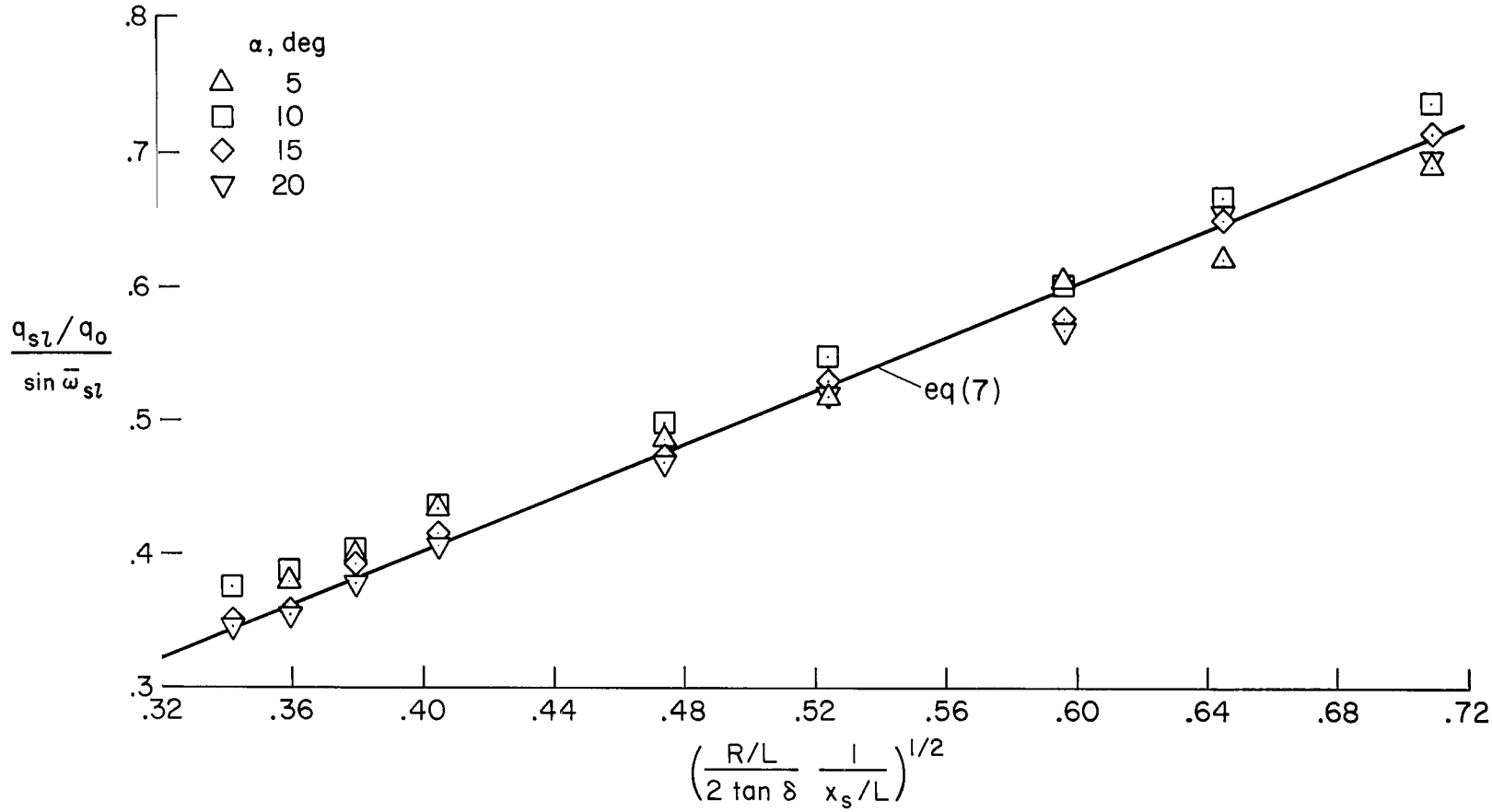

Figure 8.- Comparison of stagnation-line heating rates with simple sweep theory; $R\hat{e}^*_\infty = 1.2\times10^6$ per foot, $\bar{\omega}_{sl} = \alpha + \delta - 5°$, $R/r_b = 0$.

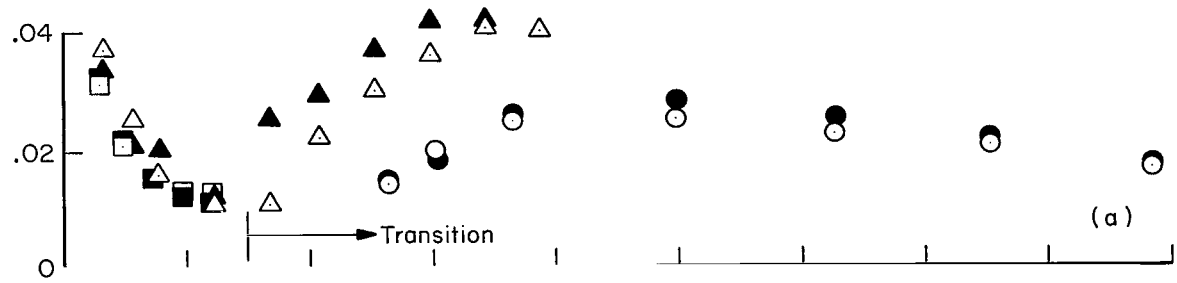

(a) $\phi = 0°$

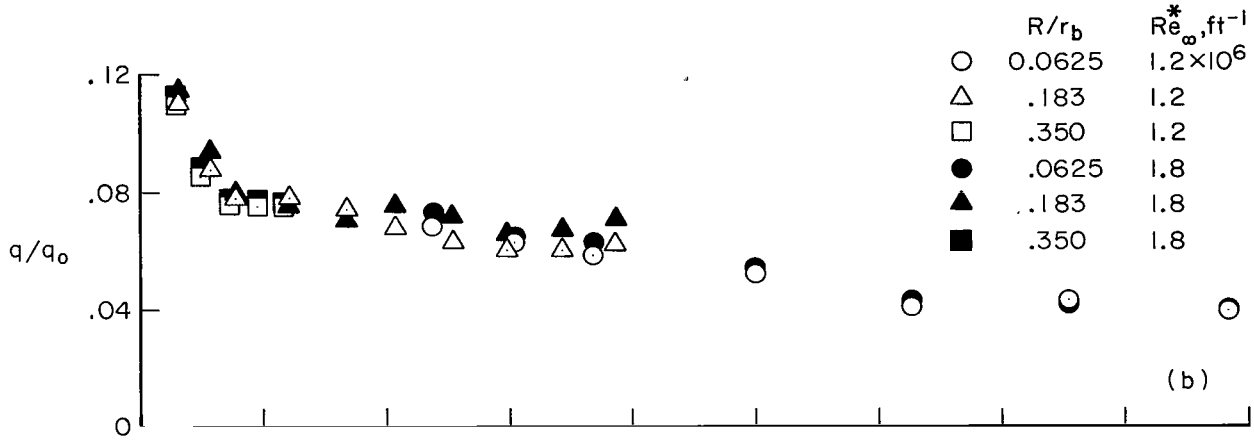

(b) $\phi = 90°$

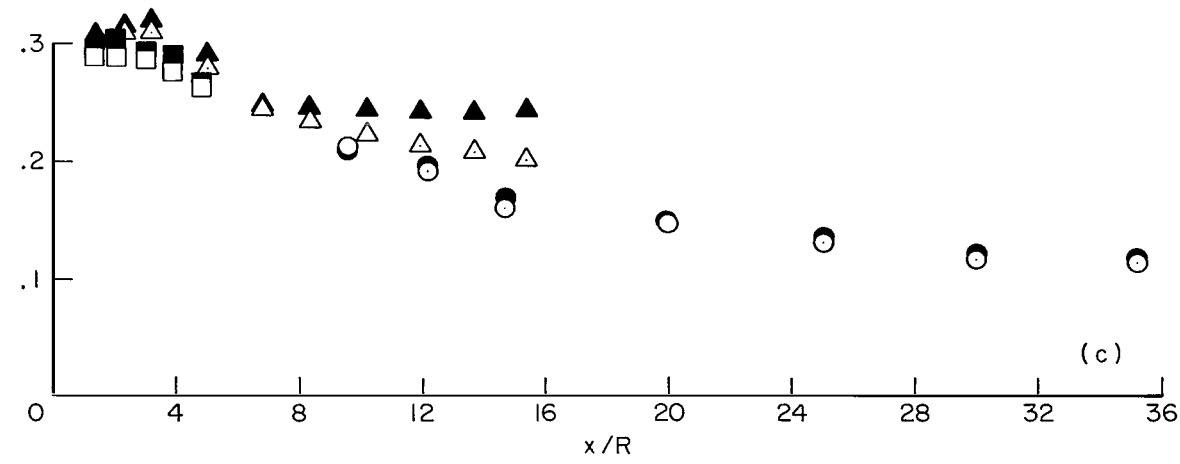

(c) $\phi = 180°$

Figure 9.- Correlation of blunt-cone heating rates; $M_\infty = 10.6$, $\delta = 15°$, $\alpha = 20°$.

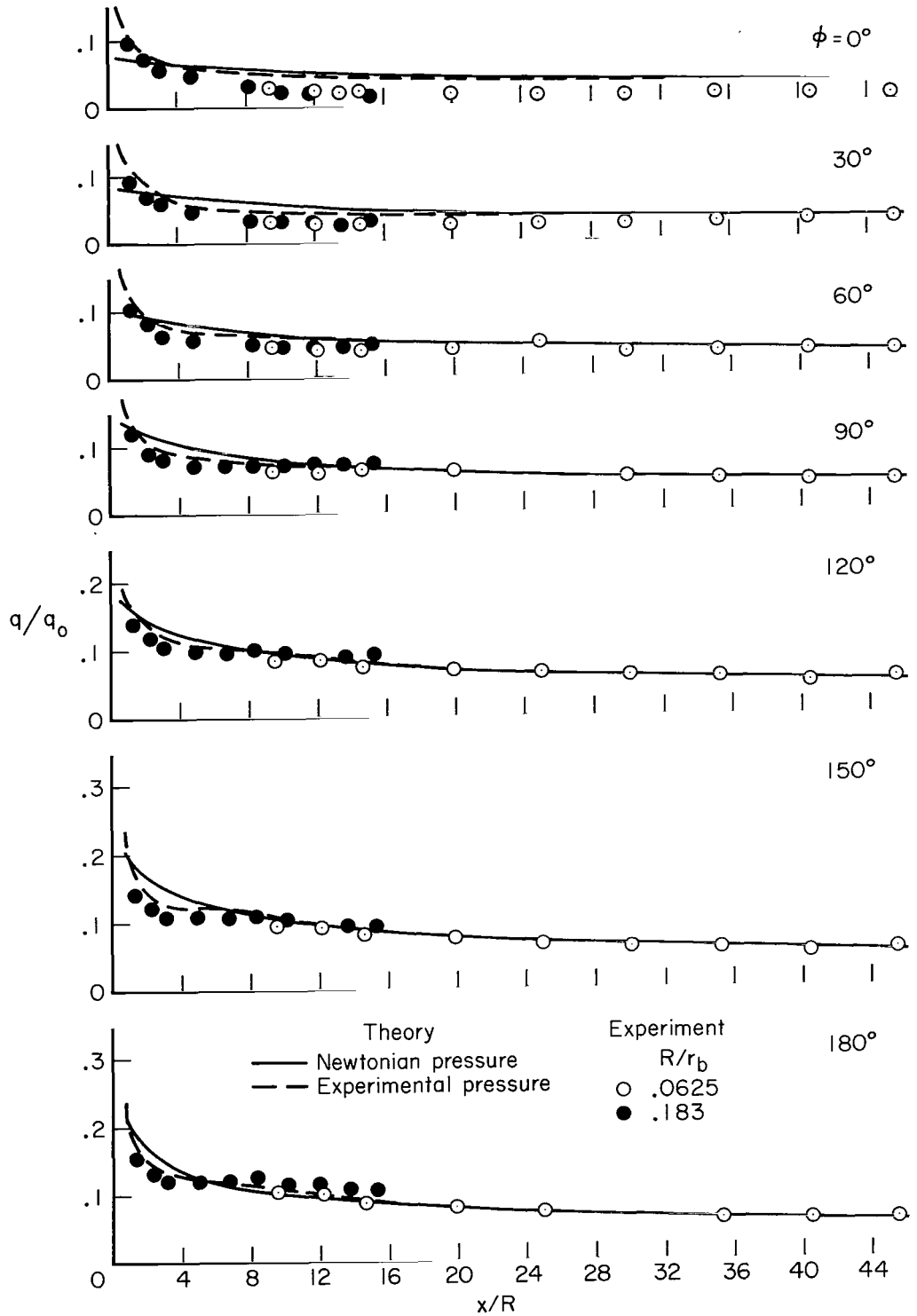

(a) $\alpha = 5°$

Figure 10.- Comparison of blunt-cone heating-rate distributions with theory for $\alpha > 0°$; $M_\infty = 10.6$, $Re^*_\infty = 1.2 \times 10^6$ per foot.

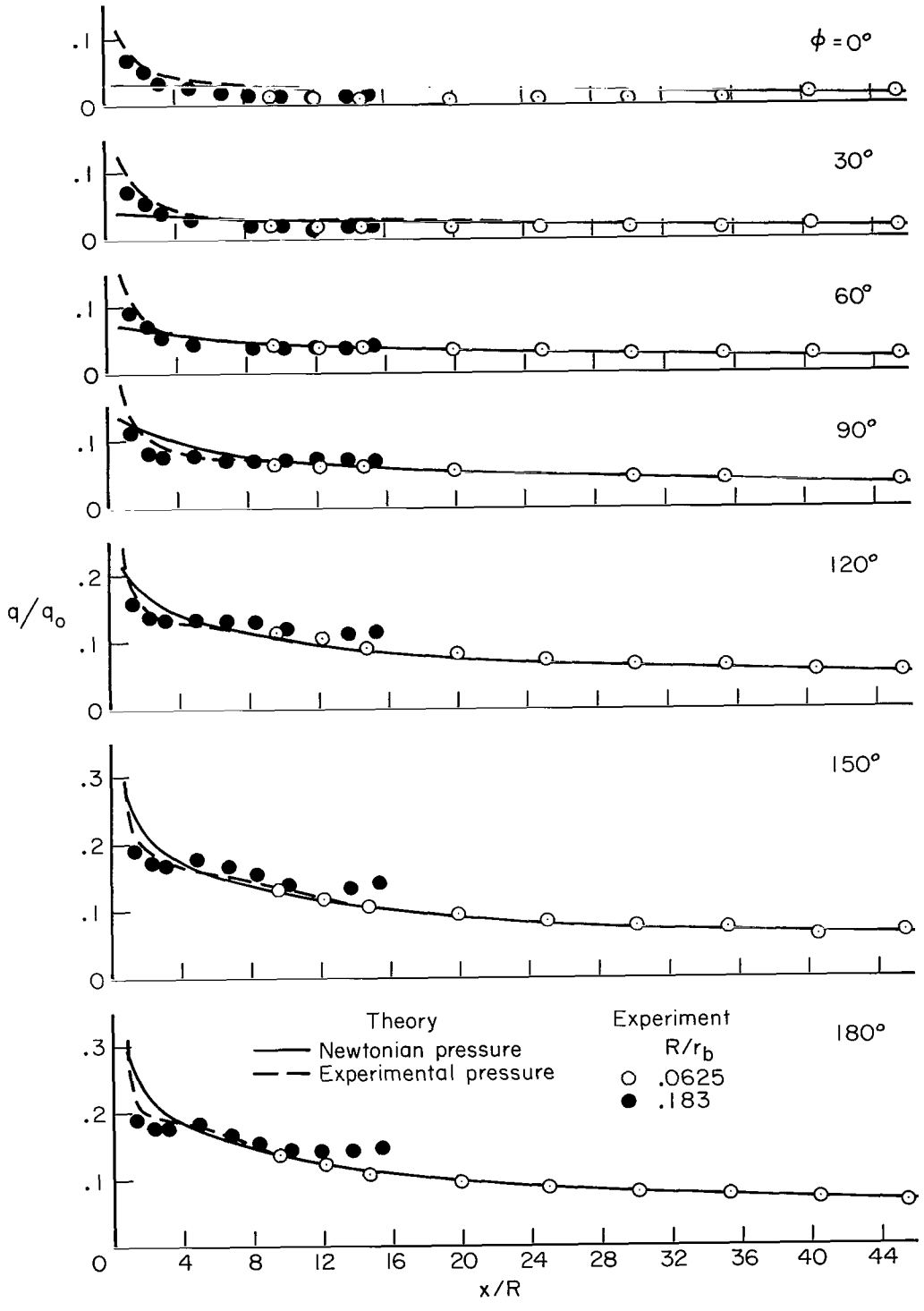

(b) $\alpha = 10°$

Figure 10.- Continued.

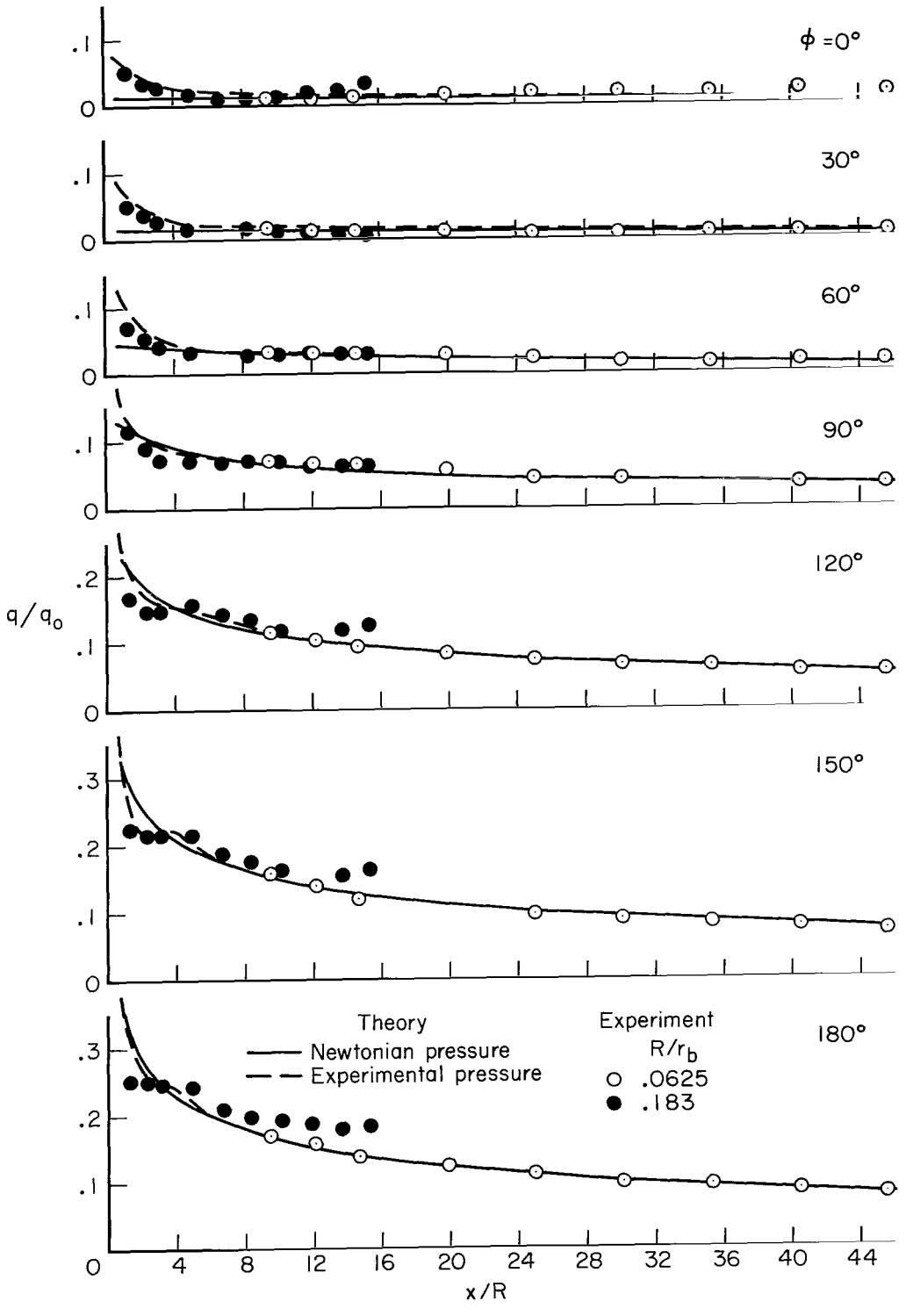

(c) $\alpha = 15°$

Figure 10.- Continued.

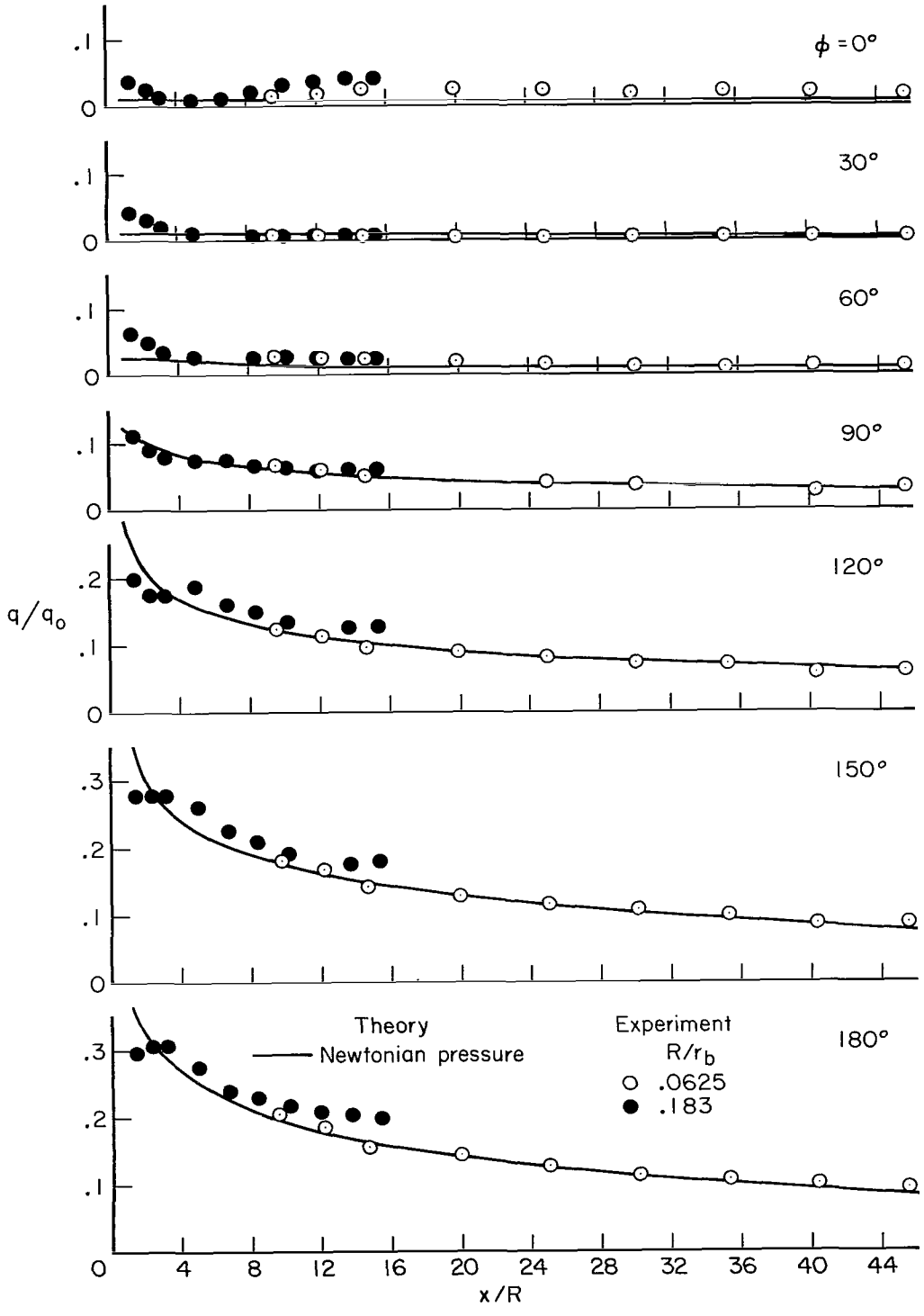

(d) α = 20°

Figure 10.- Concluded.

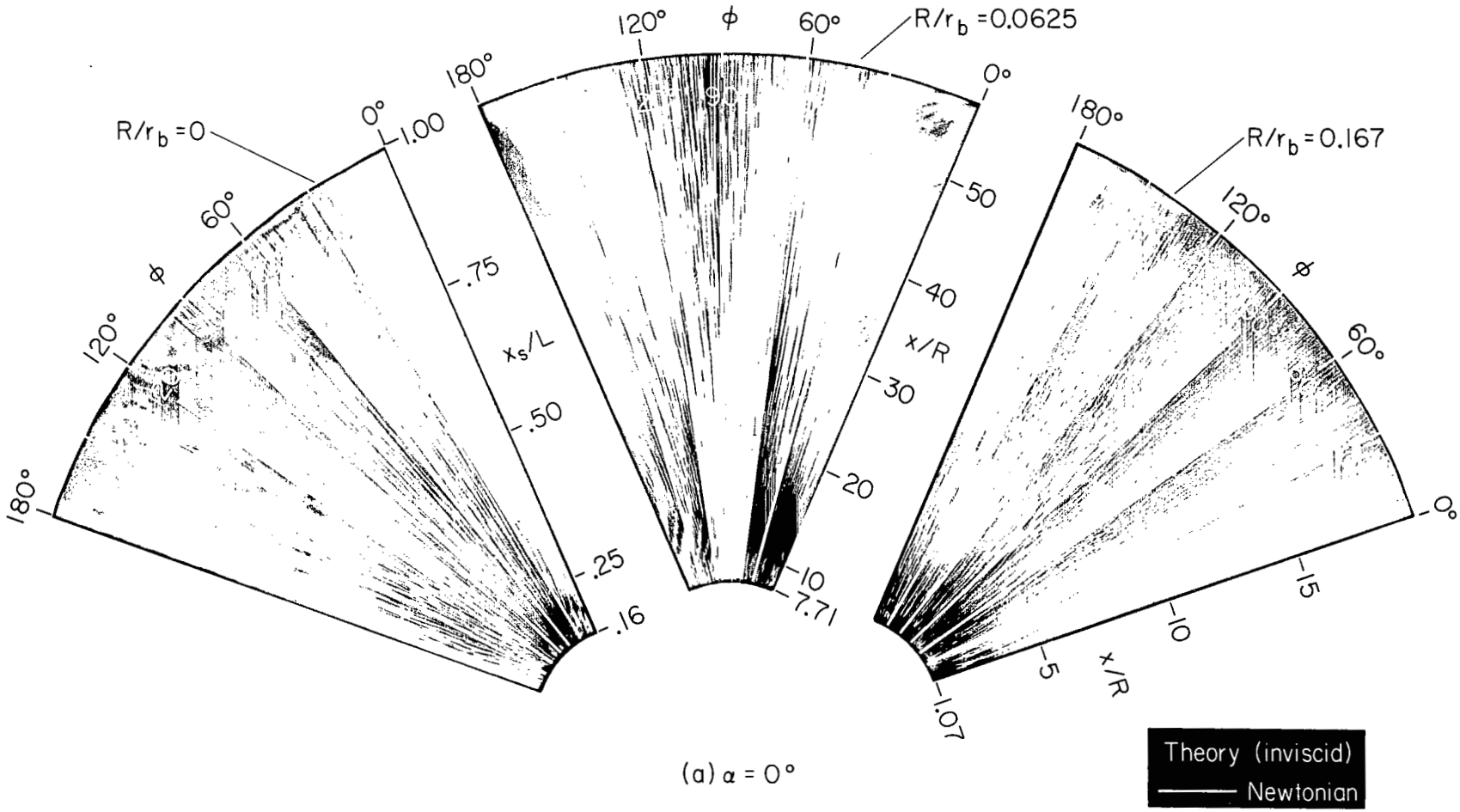

(a) $\alpha = 0°$

Figure 11.- Comparison of surface flow with inviscid theory; $M_\infty = 10.6$, $Re^*_\infty = 1.2 \times 10^6$ per foot, $\delta = 15°$.

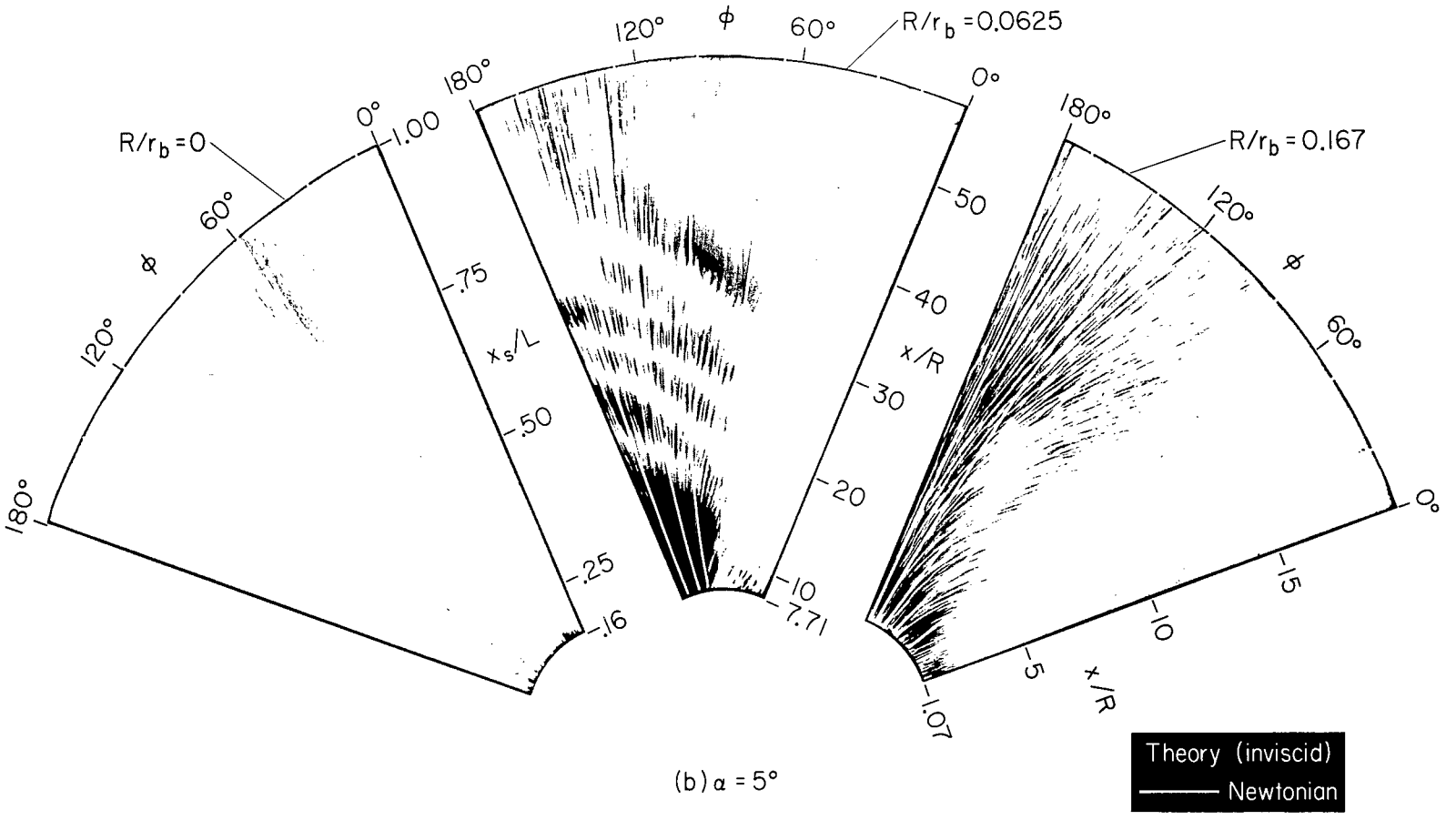

(b) $\alpha = 5°$

Figure 11.- Continued.

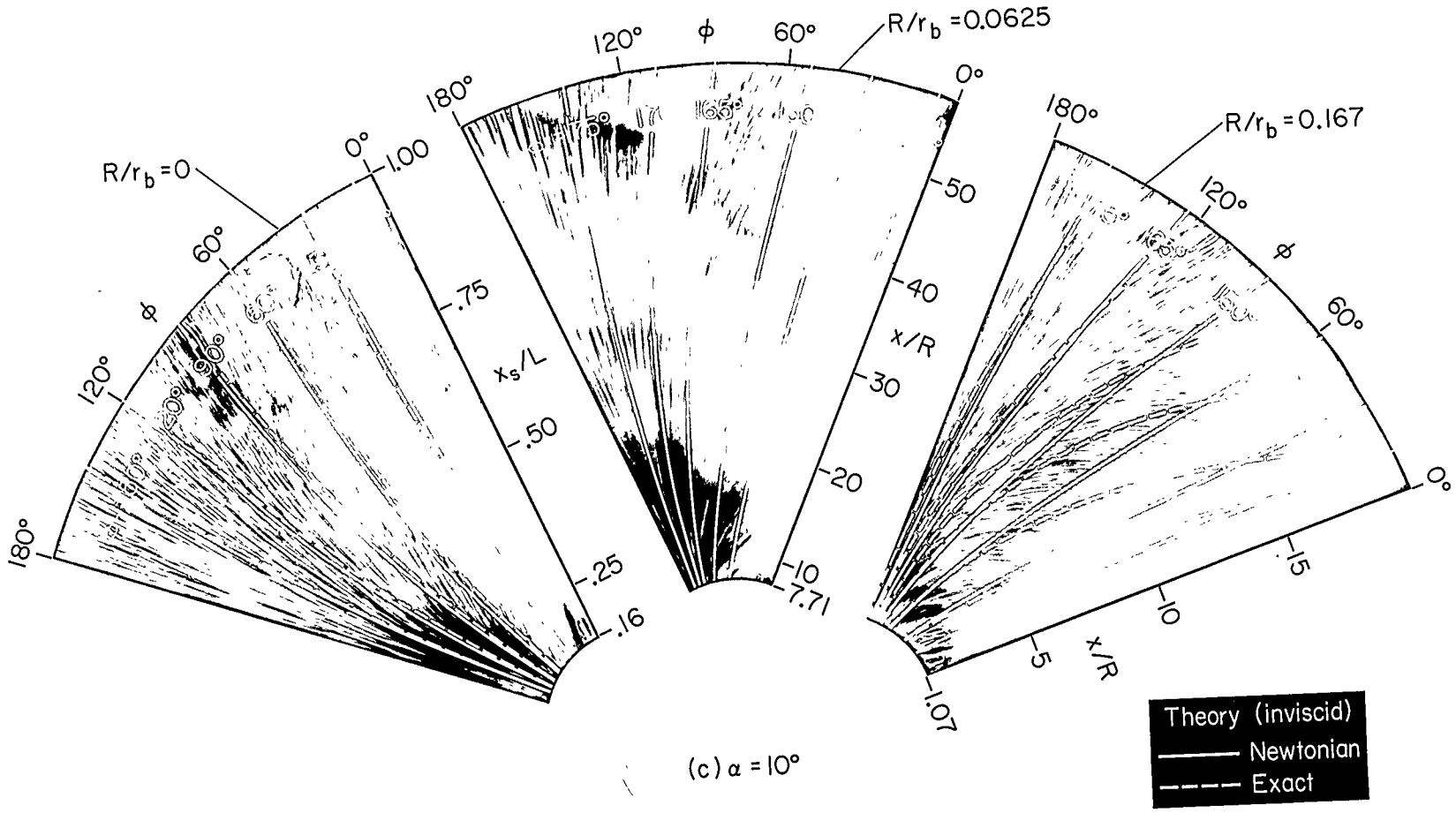

(c) $\alpha = 10°$

Figure 11.- Continued.

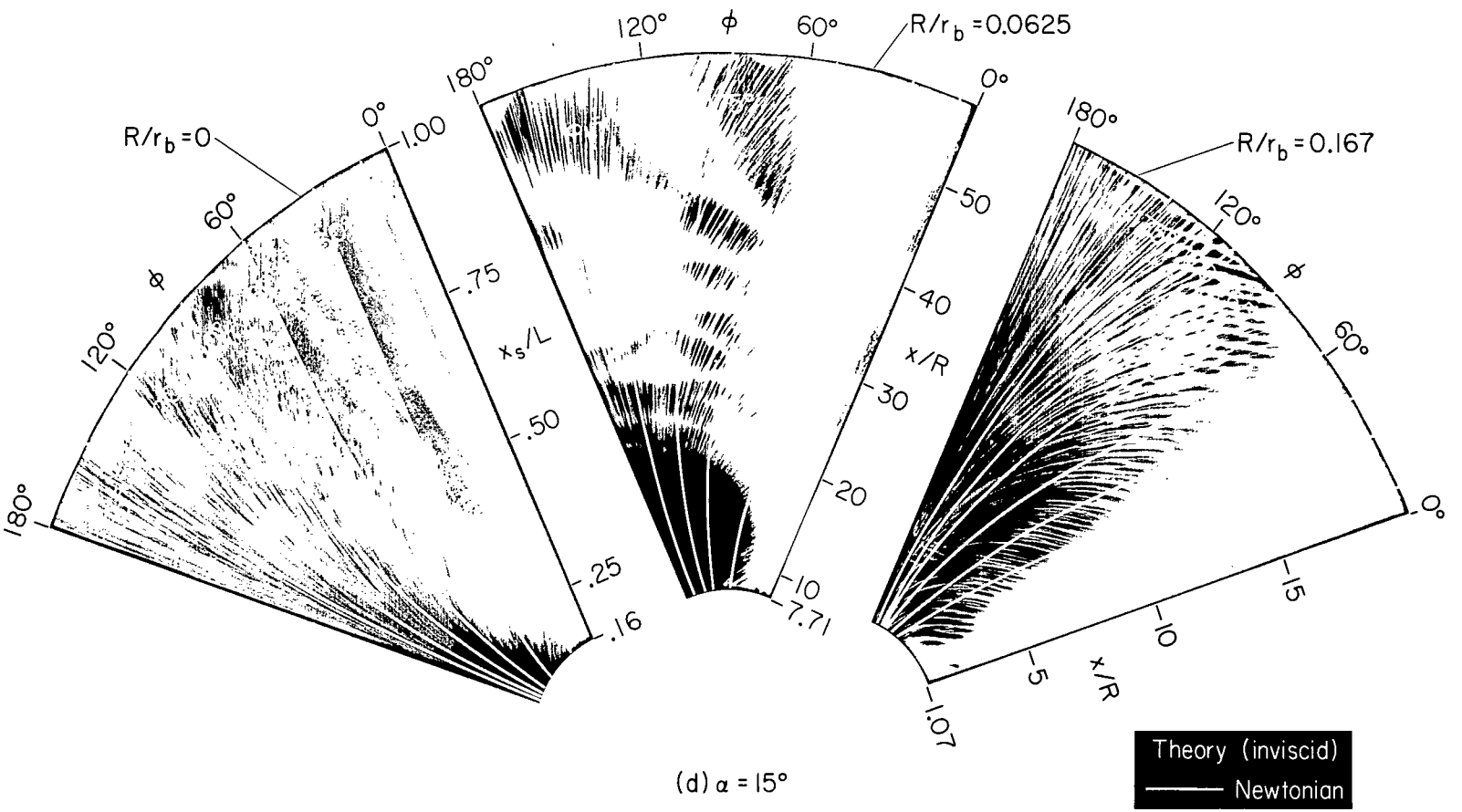

(d) $\alpha = 15°$

Figure 11.- Continued.

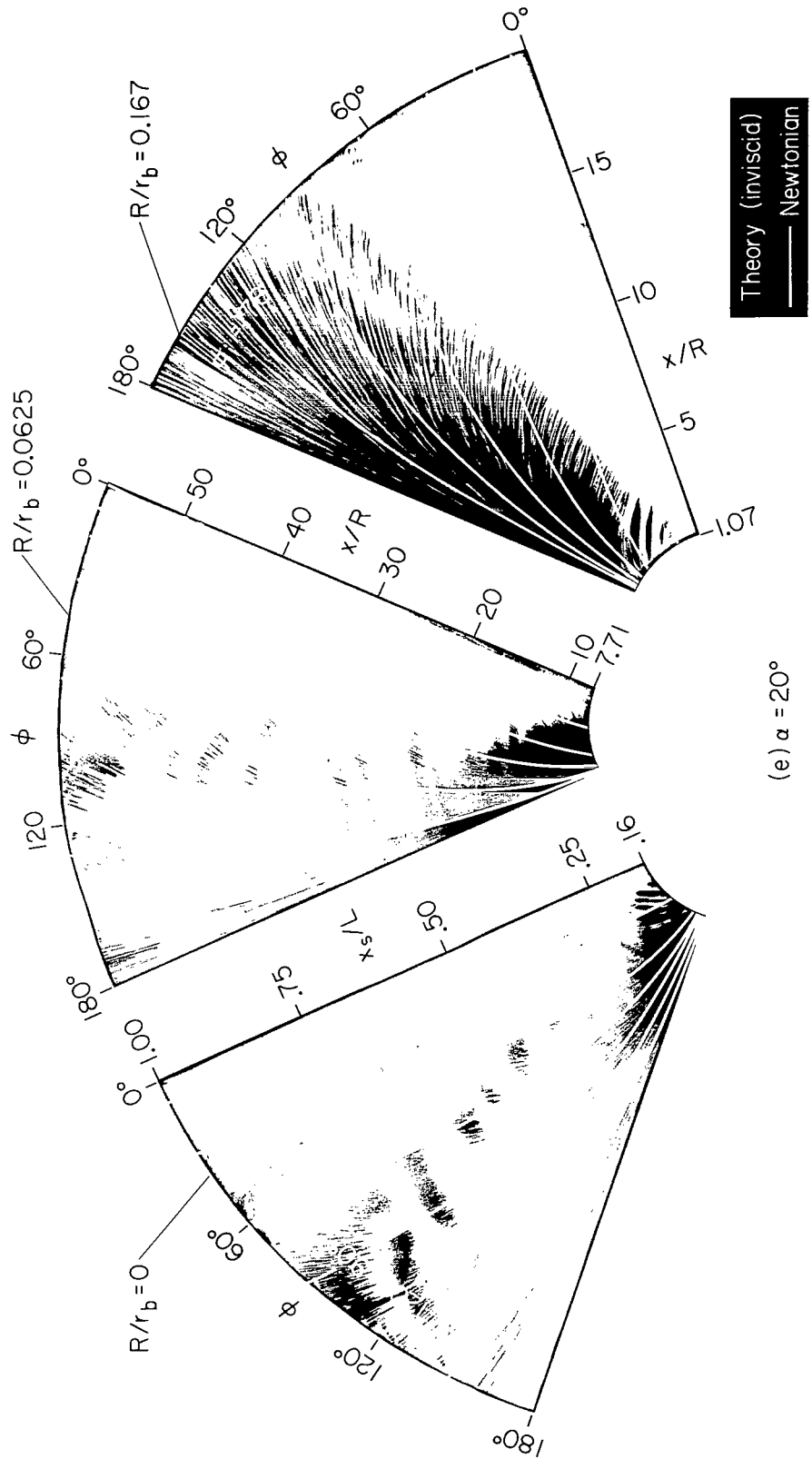

Figure 11.- Concluded.

NASA-Langley, 1969 — 12 A-3324